Performance Enhancement of Fault Ride Through of Doubly Fed Induction Generator Using Integral Terminal Sliding Mode Control

This thesis is submitted in the partial fulfilment of the requirements of the degree

MASTER OF ELECTRICAL ENGINEERING

Submitted by

Shubhranil Chakraborty

Examination Roll Number: **M4ELE22014**

Registration Number: **154004** of 2020–2021

Under the Guidance of

Dr. Debashis Chatterjee

and

Dr. Sayantan Chakraborty

Department of Electrical Engineering

JADAVPUR UNIVERSITY

KOLKATA–700032

July, 2022

Faculty Council of Engineering and Technology

Jadavpur University

Kolkata- 700032

Certificate

This is to certify that the thesis entitled "Performance Enhancement of Fault Ride Through of Doubly Fed Induction Generator Using Integral Terminal Sliding Mode Control", submitted by Shubhranil Chakraborty (Examination Roll No:- M4ELE22014), under the supervision and guidance of Dr. Debashis Chatterjee, Professor, Electrical Engineering Department, Jadavpur University and Dr. Sayantan Chakraborty, Assistant Professor, Electrical Engineering, Jadavpur University. We are satisfied with his work, which is being presented for the partial fulfilment of the degree of Master of Electrical Engineering (Control Systems) from Jadavpur University, Kolkata-700032.

Dr. Debashis Chatterjee
Professor
Department of Electrical Engineering
Jadavpur University
Kolkata-700032

Dr. Sayantan Chakraborty
Assistant Professor
Department of Electrical Engineering
Jadavpur University
Kolkata-700032

Prof. Saswati Mazumdar
Head of the Department
Department of Electrical Engineering
Jadavpur university
Kolkata-700032

Prof. Chandan Mazumdar
Dean
Faculty Council of Engineering and Technology
Jadavpur university
Kolkata-700032

Faculty Council of Engineering and Technology

Jadavpur University

Kolkata- 700032

Certificate of Approval

This is to certify that the thesis entitled "Performance Enhancement of Fault Ride Through of Doubly Fed Induction Generator using Integral Terminal Sliding Mode Control", presented by Shubhranil Chakraborty (Examination Roll No. M4ELE22014, Registration No. 154004 of 2020-21) to Jadavpur University for the partial fulfilment of the Master of Electrical Engineering(Control Systems), is hereby approved by the committee of final examination and that the student has successfully defended the thesis in the viva-voce examination.

Final examination for evaluation of thesis

Signature of Examiners

Declaration of Originality

I hereby declare that this thesis contains literature survey and original research work done by me. All the information and simulations in this document have been presented in accordance with academic rules and ethical conduct. I also declare that, as required by the academic rules and conduct, I have fully cited and referenced all papers and results that are not original to this work.

Name : SHUBHRANIL CHAKRABORTY

Examination Roll No. : M4ELE22014

Thesis Title : Performance Enhancement of Fault Ride Through of Doubly Fed Induction Generator Using Integral Terminal Sliding Mode Control

Signature with Date :

Acknowledgement

I express my utmost gratitude to my supervisor, Dr. Debashis Chatterjee for his encouragement, suggestion and advices, without which it would not have been possible to complete my thesis successfully. I would also like to thank Dr. Sayantan Chakraborty for being a constant source of encouragement, inspiration and for his valuable suggestions coupled with their technical expertise throughout my research work. It was a great honour for me to pursue my research under their supervision. Moreover, I also would like to express my gratitude to of all my co-workers including Suman Kundu, Aritra Pal, Sk Nasim Ali, all the staffs and PhD Scholars of Electric Drives Laboratory for providing constant encouragement and useful materials throughout my thesis work. Last but not the least I would like to express my love and gratitude to my parents for personally motivating me to carry out the work smoothly.

Contents

Abstract…….... ix

List of acronyms…...…….... x

List of figures…….... xi

List of tables……..... xv

Chapter 1: Introduction…..... 1

1.1. Introduction to Wind Energy Conversion System…..... 1
1.2. Introduction to Doubly Fed Induction Generator…..... 2
1.3. Working Principal of DFIG……... 3
1.4. Work Objective……..... 5
1.5. Thesis Organisation…… 6

Chapter 2: Literature Review for Different Low Voltage Ride Through Techniques……. 7

2.1. Introduction…… 7
2.2. Auxiliary hardware Based Approach…..... 7
2.2.1. Dynamic Voltage Restorer…… 7
2.2.2. Static Synchronous Compensator…… 8
2.2.3. Nine Switch Converter…….. 8
2.2.4. Crowbar……. 9
2.2.5. Series Grid Side Converter……... 9
2.3. Software based approach…… 9
2.3.1. Conventional PI Control……... 10
2.3.2. Virtual Damping Flux Based approach……. 10
2.3.3. Feedforward Current Reference Approach……..…… 10
2.3.4. Inductance Emulating approach……... 11
2.3.5. Sliding Mode Control Approach……... 11

2.4. Flowchart of Existing FRT Techniques…….. 12
2.5. Chapter Summary……... 13

Chapter 3: Introduction to Integral Terminal Sliding Mode Approach…… 14

3.1. Introduction…..... 14
3.2. Revision of Sliding Mode Control…….. 14
3.2.1. Mathematical Approach of Sliding Mode Control…… 15
3.2.2. Convergence Condition for Sliding Mode Control…..... 15
3.2.3. Equivalent Control law generation for Sliding mode Control…..... 17
3.3. Introduction to Terminal Sliding mode Control…..... 19

3.4. Introduction to Integral Terminal Sliding Mode Control……... 19
3.4.1. Mathematical Formulation of Integral Terminal Sliding mode control in nonlinear system…… 20
3.5. Chapter Summary……... 21

Chapter 4: Mathematical Derivation for Grid Connected DFIG based WECS System……... 22

4.1. Introduction…… 22
4.2. Mathematical Modelling of wind turbine……... 22
4.3. Mathematical modelling of DFIG……... 23
4.3.1. Mathematical Modelling of DFIG Stator and Rotor……. 23
4.3.2. Mathematical Modelling of back-to-back PWM converter…….. 26
4.4. Clarke and Park Transformation……. 28
4.5. Angle Estimation…… 29
4.6. Control Implementation for Conventional PI controller……. 29
4.6.1. Rotor Side Converter Control Implementation…… 31
4.6.2. Grid Side Converter Control Implementation…….. 33
4.7. Control Implementation for Sliding Mode controller……. 34
4.7.1. Rotor Side Converter Control Implementation……. 34
4.7.2. Grid Side Converter Control Implementation……... 37
4.8. Control Implementation for Integral Terminal Sliding Mode controller…… 40
4.8.1. Rotor Side Converter Control Implementation……. 40
4.8.2. Grid Side Converter Control Implementation……... 42
4.9. Chapter Summary……... 44

Chapter 5: Simulations…… 45

5.1. Introduction…… 45
5.2. Model Description of DFIG…… 45
5.3. Wind Turbine Block description……. 47
5.4. Simulation Test Condition and Results……... 49
5.4.1. Fault Ride through Check using Conventional PI Controller……... 50
5.4.2. Fault Ride through Check using Sliding mode Controller…… 51
5.4.3. Fault Ride through Check using Integral Terminal Sliding mode Controller……... 53
5.5. Result Summary…….. 55
5.5.1. Data Comparison…….. 55
5.6. Insertion of Crowbar……... 57
5.6.1. Fault Ride through Check using Sliding mode Controller with crowbar…….. 57
5.6.2. Fault Ride through Check using Integral Terminal Sliding mode Controller with crowbar…… 60
5.7. Result Summary…….. 62
5.7.1. Data Comparison…….. 62
5.8. Chapter Summary……... 64

Chapter 6: Conclusion and Future Work…….. 65
6.1. Conclusion…..... 65

6.2. Future Work…… 65

Reference……... 67

Abstract

This thesis focuses on the fixed speed application of the Doubly Fed Induction Generator (DFIG). The objective of this thesis is to develop a grid fault tolerant control of DFIG. For this, a nonlinear robust control methodology (Integral Terminal Sliding Mode Control) is been presented to mitigate the effects of grid fault. The design is based on a novel sliding manifold to reduce the chattering effect that is shown in the so called first order sliding mode control.

The controller performance and its robustness were studied under voltage sag conditions and parameter variations. Simulation results, carried out using realistic scenarios, confirmed the system robustness against parameter variations and its effectiveness in mitigating voltage sags. The performance of the proposed approach was further compared to that of a standard SMC approach and conventional PI controller-based approach in terms of voltage sag mitigation abilities and chattering alleviation. While both SMC approaches were able to mitigate the effects of voltage sags and protect the rotor circuit against over-currents, the proposed ITSMC was shown to be more effective than CSMC and PI based approach in mitigating deep voltage sags and reducing the chattering effect. Furthermore, the analysis of the crowbar protection system to protect the system under symmetrical voltage dips is also performed.

List of acronyms

P_m = Mechanical Power Generated by Wind Turbine

P_s = Stator Active Power of Doubly Fed Induction Generator

P_r = Rotor Active Power of Doubly Fed induction Generator

Q_s = Stator Reactive Power of Doubly Fed Induction Generator

Q_r = Rotor Reactive Power of Doubly Fed Induction Generator

T_m = Mechanical Torque generated by wind turbine

ω_s = Rotational speed of synchronously rotating frame

ω_r = Rotating Speed of Rotor

R_s = Stator Resistance

R_r = Rotor Resistance

L_s = Stator Inductance

L_r = Rotor Inductance

L_m = Mutual Inductance

I_{ds}, I_{qs} = Direct and quadrature axis current of Stator

I_{dr}, I_{qr} = Direct and quadrature axis current of Rotor

V_{ds}, V_{qs} = Direct and quadrature axis voltage of Stator

V_{dr}, V_{qr} = Direct and quadrature axis voltage of Rotor

I_{df}, I_{qf} = Direct and quadrature axis current of Grid Filter current

V_{dg}, V_{qg} = Direct and quadrature axis current of Grid Voltage

$\lambda_{ds}, \lambda_{qs}$ = Stator and Rotor axis flux

T_{em} = Electromagnetic Torque generated by the machine

J = Moment of Inertia of wind turbine

s = Sliding surface

List of figures

Figure 1.1: Block diagram of a typical wind turbine connected Doubly fed induction generator…….……2

Figure 1.2: Block diagram of a Doubly fed induction generator connected to the grid……...4

Figure 1.3: Grid Codes in Different Countries for Fault Ride Through……....6

Figure 3.1. Sliding Condition……...16

Figure 3.2. Sliding Surface and Chattering phenomenon……18

Figure 4.1. dq axis circuit diagram of Doubly fed Induction generator……...24

Figure 4.2. Schematic diagram of back-to-back converter……..26

Figure 4.3. Phasor diagram of dq to abc conversion……28

Figure 4.4. Current control loop of Rotor side converter with Conventional PI control……..32

Figure 4.5. Current control loop of Grid side converter with Conventional PI control……..33

Figure 4.6: Control Implementation of Rotor Side Converter with SMC approach……..37

Figure 4.7: Control Implementation of Grid Side Converter with SMC approach……..39

Figure 4.8: Control Implementation of Rotor Side Converter with ITSMC approach……..42

Figure 4.9: Control Implementation of Grid Side Converter with ITSMC approach……..44

Figure 5.1. MATLAB/SIMULINK Block diagram for simulation of
fault ride through with different controllers……46
Figure 5.2. Wind Turbine Power Characteristics……49
Figure 5.3: Grid voltage waveform with fault applied…….....49
Figure 5.4: Normal value of Stator current…….....49
Figure 5.5: Normal value of Rotor current…….....49
Figure 5.6.1: Stator Current Variation in Conventional PI Controller……50
Figure 5.6.2: Rotor Current Variation in Conventional PI Controller……50
Figure 5.6.3: Stator Active Power Variation in Conventional PI Controller..….....51
Figure 5.6.4: Stator Reactive Power Variation in Conventional PI Controller.…..51
Figure 5.6.5: Torque Variation in Conventional PI Controller……...51
Figure 5.7.1: Stator Current Variation in Sliding mode Controller…….....52
Figure 5.7.2: Rotor Current Variation in Sliding mode Controller…….....52
Figure 5.7.3: Stator Active Power Variation in Sliding mode Controller…….....52
Figure 5.7.4: Stator Reactive Power Variation in Sliding mode Controller…..…..52
Figure 5.7.5: Torque Variation in Sliding mode Controller…….…..53
Figure 5.8.1: Stator Current Variation in Integral Terminal Sliding
mode Controller…….53
Figure 5.8.2: Rotor Current Variation in Integral Terminal Sliding
mode Controller…….54
Figure 5.8.3: Stator Active Power Variation in Integral Terminal
Sliding mode Controller…….54
Figure 5.8.4: Stator Reactive Power Variation in Integral Terminal
Sliding mode Controller…….54

Figure 5.8.5: Torque Variation in Integral Terminal Sliding
mode Controller……..54
Figure 5.9. Crowbar Circuit……57
Figure 5.10.1: Stator Current Variation in Sliding mode Controller
with Crowbar……..58
Figure 5.10.2: Rotor Current Variation in Sliding mode Controller
with Crowbar……..58
Figure 5.10.3: Stator Active Power Variation in Sliding mode Controller
with Crowbar……..58
Figure 5.10.4: Stator Reactive Power Variation in Sliding mode Controller
with Crowbar……..58
Figure 5.10.5: Torque Variation in Sliding mode Controller
with Crowbar……..59
Figure 5.10.6: Crowbar Current in SMC approach…….……...59
Figure 5.11.1: Stator Current Variation in Integral Terminal Sliding
mode Controller with Crowbar…….....60
Figure 5.11.2: Rotor Current Variation in Integral Terminal Sliding
mode Controller with Crowbar…….....60
Figure 5.11.3: Stator Active Power Variation in Integral Terminal Sliding
mode Controller with Crowbar…….....60
Figure 5.11.4: Stator Reactive Power Variation in Integral Terminal
Sliding mode Controller with Crowbar…….. 61
Figure 5.11.5: Torque Variation in Integral Terminal Sliding mode

Controller with Crowbar…….61

Figure 5.11.6: Crowbar Current in ITSMC approach…….61

List of tables

Table 5.1: Doubly Fed Induction generator and grid parameter values……46
Table 5.2: Wind turbine parameters……..48
Table 5.3: Comparison of Stator current transient characteristics in 3 different controllers……..56
Table 5.4: Comparison of Rotor current transient characteristics in 3 different controllers……..56
Table 5.5: Comparison of Active Power transient characteristics in 3 different controllers……..56
Table 5.6: Comparison of Reactive Power transient characteristics in 3 different controllers……..57
Table 5.7: Comparison of Torque transient characteristics in 3 different controllers……..57
Table 5.8: Comparison of Stator current transient characteristics in 2 different controllers with crowbar……62
Table 5.9: Comparison of Rotor current transient characteristics in 2 different controllers with crowbar……62
Table 5.10: Comparison of Active Power transient characteristics in 2 different controllers with crowbar……63
Table 5.11: Comparison of Reactive Power transient characteristics in 2 different controllers with crowbar……63
Table 5.12: Comparison of Torque transient characteristics in 2 different controllers with crowbar……..63

Chapter 1

Introduction

1.1. Introduction to Wind Energy Conversion System (WECS):

Wind power generation is a promising way of energy generation in the renewable energy market for their cleanliness, inexhaustible source, and a replacement of non-renewable energy sources. The wind energy generation, as the name suggests, is produced by the help of wind flow. The flow of the wind rotates the wind turbine, which is coupled with an electrical generator through the shaft. Mainly squirrel cage induction generator, Permanent magnet synchronous generator or doubly fed induction generators are used as electrical generators. The output voltage of the electrical generators are coupled with power electronic circuitry in order to control the output before feeding to the grid.[1]

There are two types of wind turbines, 1. Constant speed wind turbine, 2. Variable speed wind turbine. In the case of fixed speed wind turbine, the wind speed remains constant so rotor of the induction machine tends to rotate in a constant speed. On the other hand, in the case of the variable speed wind turbine, rotational speed is changed in response to wind speed changes so that the C_p(Betz limit) can be kept at its maximum limit. We shall discuss more about C_p in Chapter 4.

When the wind speed increases, the output power of the generator increases as a function of the rotational speed. Maximum Power point tracking algorithm and pitch angle control can be used to extract maximum power from WECS and maintain stability in the system.

Among all types of Renewable energy sources, Wind energy are being used significantly for many years. Among renewable energy sources, the application of wind energy is fastest going and it tends to increase more in future. The increased penetration of wind energy-based electricity production creates new challenges for the power system operators to ensure reliable and safe grid operation. There are different grid codes for different countries, and some countries also are revising their grid codes in order to maintain safety and reliability, such as in Denmark and Germany [2,3]. Grid codes are basically a rule of connection and disconnection periods of DFIG for a certain type of fault, depending upon the voltage dip.

The system to convert the energy present in the wind to useful form of energy is known as Wind Energy Conversion system (WECS). In the past, the wind power was utilised in the form

of useful mechanical power but in modern world WECS is mainly concentrated on conversion of energy to electrical form to supply a certain area. The conversion of the wind energy into the electrical energy depends on different factors like Wind speed, blade length, turbine type, etc. [4].

Wind energy systems are complex structures driven by random wind flow disturbances, gravitational, and gyroscopic loads. Although Squirrel cage induction generator and Permanent magnet Synchronous generators are used, Doubly Fed Induction Generator (DFIG)-based wind turbines (WT) are the most common type of Asynchronous Induction generators that are used in wind energy conversion system. However, wind turbine's direct connection to the grid has led to new control challenges in voltage sag conditions. The voltage dip condition is a reduction in rms line voltage of grid for a short duration of time which can be caused by a short circuit, overload, or starting of electric motors. A voltage sag typically happens when the rms voltage decreases more than 50 percent of its nominal value for a significant duration of time. Voltage dips effect in short-duration increase in currents—the higher the voltage sag magnitude, the higher the fault current. Hence, during voltage sags, the current of the DFIG's rotor increases considerably. It is worth noting that controlling the rotor side converter (RSC) and grid side converter (GSC) alone during grid faults will not prevent WT's disconnection from the grid, especially when the fault magnitude is significant (deep voltage sags). Note that even the smallest variations in grid voltages can lead to severe damages to the wind turbine's converters, if the control approaches are not designed considering such disturbed grid voltage profiles. Hence, any fault ride-through (FRT) design should be augmented by additional controllers or components to ensure the continuous connectivity of the wind turbine to the grid regardless of fault magnitude. This chapter will discuss the contributions of this work to the FRT of DFIG-based wind turbines.

1.2. Introduction to Doubly fed Induction Generator:

Doubly Fed Induction Generators are widely used in Wind energy conversion system. This type of generators are basically a type of induction generator, here the Stator side is connected to the grid (Utility grid or microgrid) directly, whereas the rotor is also connected to the grid with the help of a back to back converter, where in between the rectifier and inverter side, there is a DC link capacitor which provides the reactive power. This type of configuration is helpful to make a smoother control of active and reactive power.

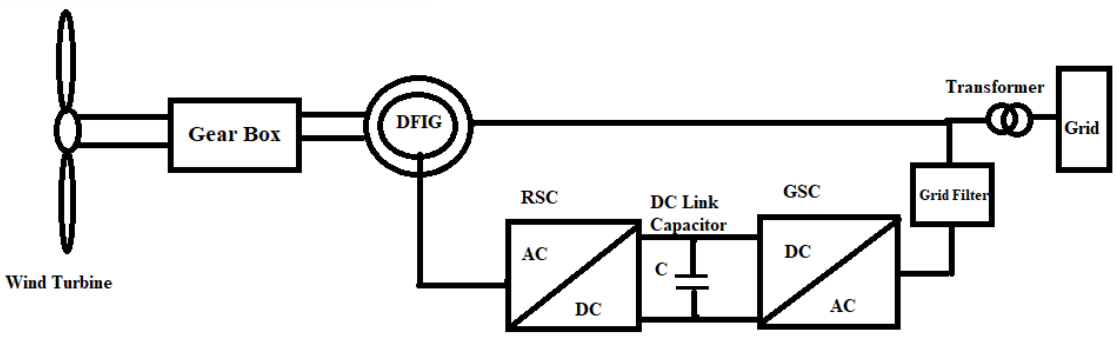

Figure 1.1: Block diagram of a typical wind turbine connected Doubly fed induction generator [5]

The figure represents the block diagram of a typical wind turbine connected Doubly fed induction generator. The wind turbine is connected to the doubly fed induction generators with the help of a gearbox. As previously mentioned, the stator is connected with the grid side and the rotor is connected to the grid with the help of a back-to-back converter. The dc link capacitor is placed between the midway of two converters. The chopper is used for overvoltage protection during voltage dip, and the crowbar circuit is connected across rotor in order to make overcurrent protection during fault period.

1.3. Working Principal of DFIG:

An induction generator is composed by a stator and a rotor. In the case of a DFIG, both stator and rotor have three sinusoidally distributed windings, corresponding to three phases, displaced by 120°. The three phases are called a, b and c. The stator has p pairs of poles. The rotor is connected to the grid through converters. A three-winding transformer gives different voltage levels for stator and rotor side. A schematic of such a system is presented in figure 1.2. When the machine produces energy, only a small part of the generated power flows from the rotor to the grid. The converters can then be chosen in accordance with this small rotor power. This means smaller converters compared to fully rated converters and this allows to decrease the costs. [6]

The stator windings are connected to the grid, so the stator current frequency is equal to the grid frequency (50 Hz). The stator currents create a rotating magnetic field in the air gap. The rotational speed of this field ω_s can be written as:

$$\omega_s = 2\pi f_s \qquad \text{(i)}$$

Since DFIG is an asynchronous machine, the rotor rotates at a different speed than the speed of rotational field or synchronous speed, Therefore, by Faraday's law of induction, currents are induced in the rotor windings.

The DFIG machine operates usually as a generator if $\omega_r > \omega_s$ and as a motor otherwise. In the case of the DFIG however, it can operate in sub-synchronous mode as a generator. The slip, s can be expressed as relative speed of the rotor compared with that of the stator

$$s = \frac{\omega_s - \omega_r}{\omega s} \quad \text{(ii)}$$

The slip is usually negative for a generator and positive for a motor. The currents induced in the rotor windings pulse at an angular speed defined by the difference between the synchronous speed and the rotor speed. From the rotor end, as the rotor speed is ω_r, it can be observed that the rotating magnetic field created by the stator pulsating at $\omega_s - \omega_r$ radian/sec. So, frequency of the rotor currents,

$$f_r = sf_s \quad \text{(iii)}$$

If the rotor is made to rotate the synchronous speed, no rate of change of magnetic flux will occur and no currents would then be induced in its windings, that results in no torque, and the machine will refuse to start. Therefore, the DFIG is made to operate always at speeds different from synchronous speed. The rotor-side inverter controls the rotor currents. From (iii), it can be said that controlling the rotor currents controls the slip and the speed of the machine.

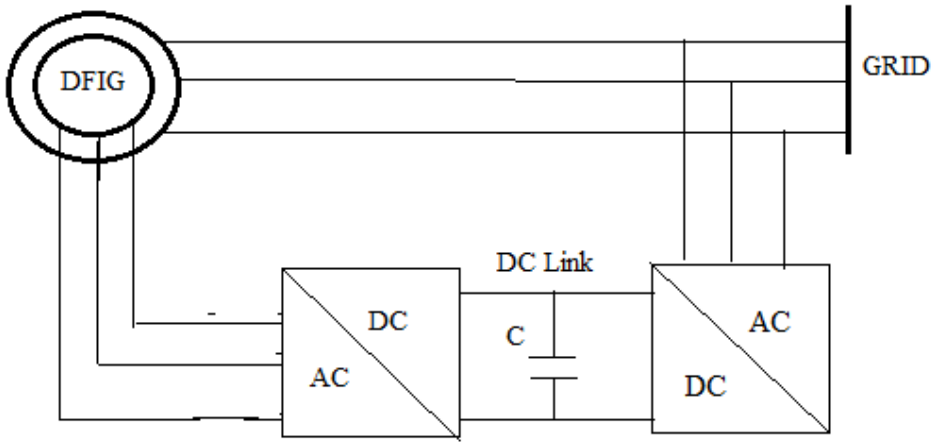

Figure 1.2: Block diagram of a Doubly fed induction generator connected to grid [6]

1.4. Work Objective:

Fault occurrence is a very typical phenomenon in Doubly fed Induction generator connected wind turbine. DFIG is extremely sensitive to grid voltage disturbance, since its stator terminal is directly connected to the grid. For instance, when the grid faults occur, large electromotive force (EMF) will be induced in the rotor circuit of DFIG, which usually far exceeds the DC-bus voltage. Therefore, it may cause overcurrent of the rotor-side converter (RSC) and overvoltage. Of the DC-bus if no effective protection scheme is adopted According to the grid codes which are followed by different countries, the DFIG should be connected to the grid for a certain period during the fault period. After that they should be disconnected from the grid. A typical grid code is displayed in the following figure.

There can be two types of grid faults. 1.Symmetrical, 2. Unsymmetrical. Symmetrical grid faults are very common in DFIG connected wind turbines and it causes significant voltage drop that may damage the system components if not addressed suitably.

To ensure that the fault effects are mitigated while DFIGs are connected according to the grid codes, different control techniques using software as well as hardware-based approaches are undertaken in many literatures. The discussion of different techniques of fault control paradigm has been discussed in the chapter 2 itself.

The main objective of this work is to diminish the transients in a quick succession in order to meet the grid codes. For this, we have presented a novel Integral terminal Sliding mode control which is a bit advanced version of normal sliding mode control. In conventional 1^{st} order type sliding mode control, the convergence condition is guaranteed in terms of asymptotic stability. Means the system will reach to its stable position, but in infinite time. In Integral Terminal Sliding Mode Control (ITSMC), the sliding surface or sliding manifold is taken such a way that some nonlinear terms are used in its equation and the manifold acts as a terminal attractor, that drags the system response to its convergence in a finite time, also integral error function helps to eliminate the singularity condition, which is a problem in Terminal Sliding mode control (TSM).

Furthermore, we also introduce a crowbar in the system in order to bypass some amount of rotor currents during fault period.

.

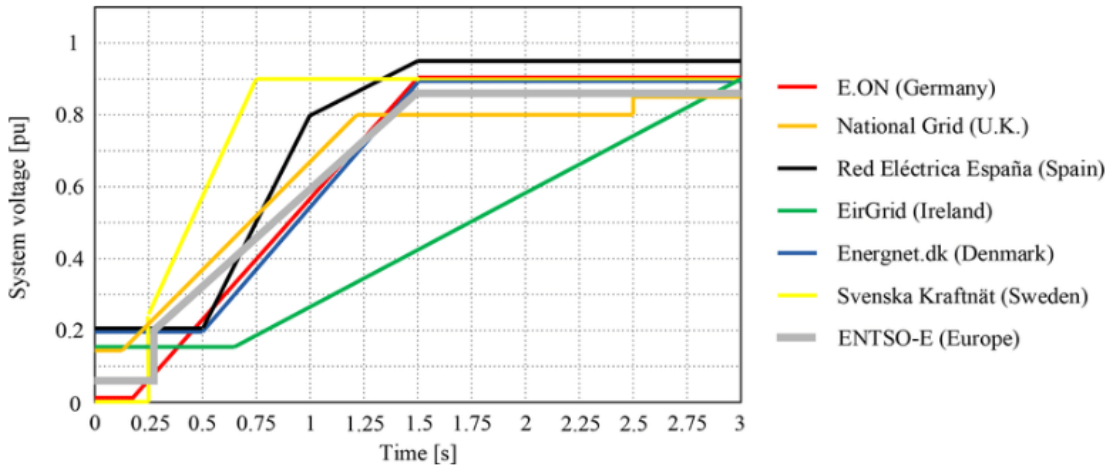

Figure 1.3: Grid Codes in Different Countries for Fault Ride Through [8]

1.5. Thesis Organisation:

The structure of the thesis is based on our work objectives mentioned above. In chapter 2, we have discussed some previous works based on Fault Ride Through techniques. The ITSMC based control approach with a complete discussion of Sliding mode control has been discussed is detailed in chapter three. Chapter 4 discusses about mathematical formulation of the system. The simulation results with conventional PI control, sliding mode control and proposed ITSMC based control with crowbar is discussed in chapter 5. Chapter six concludes this dissertation with the summary of contributions and suggestions of future work.

Chapter 2

Literature Review of Existing FRT technique

2.1. Introduction:

In this chapter, we shall discuss about different Fault ride through techniques that have been applied in previous work. In chapter 1, it is presented that the fault ride through technique in DFIG based wind turbine can be employed by 2 methods, 1. Auxiliary hardware-based method, 2. Software Based control technique. As this particular work is a combination of both hardware and software-based fault effect mitigation technique, I have mentioned the pre-existing works of the both techniques in the subsequent sections. Among these, some works have employed only Hardware based technique, some papers have employed software-based technique, and some papers have undertaken hybrid technique for fault mitigation.

2.2. Auxiliary Hardware based approach [9]:

This method is based on employing hardware circuitry in order to prevent rotor side converters and Dc link capacitors from overcurrent and overvoltage respectively. Generally, this protection scheme is implemented by bypassing the RSC by the help of a crowbar circuit. This method is low-cost and simple, but the disadvantage is that the DFIG can lose its controllability and the crowbars can absorb reactive power from the grid. To overcome this drawback, several other auxiliary hardware-based methods are proposed to achieve better transient performance, e.g., dynamic voltage restorer (DVR)[10], nine switch-converter[12], static synchronous compensator (STATCOM)[11], and series grid side converter (SGSC). [13]

2.2.1. Dynamic Voltage Restorer:

In case of a grid side fault in DFIG connected wind turbine, to mitigate the effect of voltage dip and to ensure low voltage ride through, the use of dynamic voltage restorer has been discussed in several papers. In this case, A dc voltage source is used where the voltage is converted to AC further by using a voltage source converter, and that voltage is fed to the grid in the fault condition. In normal operating mode, however, the DVR is disconnected from the grid. In [14]-[16] low voltage ride through is presented using DVR. In [17], adaptive fuzzy PI controller is used along with DFIG controller for LVRT study. The advantages of the DVR are

to reduce the control strategy complexity of the DFIG system, and to ensure the DFIG uninterrupted operation.

2.2.2. Static Synchronous Compensator (STATCOM):

Static Synchronous Compensators or STATCOM are used to provide reactive power support in the grid in order to manage low voltage ride through in the system. A STATCOM is a capacitor based shunt-connected FACTSs device that is capable of generating and/or absorbing reactive power. Usually, the STATCOM is applied to voltage support aims. Recently, a large number of wind turbines installed are the variable speed type fitted with DFIGs. Under normal operating conditions, the DFIGs operate at close to unity power factor and may supply some reactive power during system disturbances such as a three-phase fault close to the wind farm in order to meet the FRT grid code requirements. In fault period, when voltage of the grid becomes very low, The STATCOM then activates and fed reactive power to the system in order to prevent the voltage collapse. In the paper [18], the STATCOM based FRT approach is undertaken with the help of gate turn-off thyristor (GTO) based PWM converter with a dc-link capacitor.

2.2.3. Nine Switch Converter:

As we know that the back-to-back converters that are used in DFIG wind turbines, consists of 2 converters, 1. Grid side Converter, 2. Rotor Side converter. But in case of a nine-switch converter, a single converter is used to connect the rotor with the grid. It is the replacement of traditional twelve-switch back-to-back converter [11]. With the help of nine switch converter, the gird-side branch gets higher voltage to maintain dc bus steady under normal condition, and the rotor-side branch gets higher voltage to withstand the rotor-overvoltage during FRT period. The proposed system and adapted control method ensure the rating capacity of the power devices can be fully used at any time, and no extra capacity margin on the power devices is required. Unlike traditional twelve-switch B2B converter that needs some extra capacity margins or auxiliary hardware along with its normal control approach to address the FRT, the NSC is more economical because it not only protects power devices but also fulfil the Fault ride through without any auxiliary hardware. In most applications, the occurrence of high dc voltage is the major drawback of a NSC, which limits its application. In the DFIG wind power system, this high dc voltage could be properly utilized to withstand the rotor-overvoltage during the voltage dipping moment, and thus, achieves the LVRT without any additional

auxiliary circuits. The advantages of NSC hardwires in DFIG wind power system, is that it only requires nine power switches so they are economical and dc voltage can be fully utilised in either normal or FRT period, and no additional voltage margin is required [19].

2.2.4. Crowbar:

It is considered to be most fundamental type of fault ride through method, and generally is concerned about limiting the rotor overcurrent. It is basically a diode bridge where a resistance (named crowbar resistance) is connected across it. Whenever, the rotor current is increased over a certain value, the diode bridge activates and the current starts to flow through the crowbar resistance.[20],[21]. Thus, the DFIG acts as a motor and starts consuming reactive power. This is a widely used hardware topology which is used to protect the converters from high transient fault current.

2.2.5. Series Grid Side Converter:

The working principle of Series grid side converter is almost similar to the Dynamic voltage restorer, except here main objective is to protect the DC bus capacitor from overvoltage. The series converter acts as a Dynamic Voltage Restorer, improving the DFIG capability to deal with disturbances in the grid, especially symmetric and asymmetric faults. In paper [22], a series grid side converter-based approach is undertaken in order to prevent the DC bus capacitor from overvoltage and to restrict the voltage fluctuation in 0.95-1.05 pu range. The filter activation and the voltage injection are done by the help of suitable controller. However, a drawback of this scheme is to control the power during sub synchronous speeds.

2.2.6. Fault Current limiter:

This is used to limit the stator currents. It protects the doubly-fed induction generator wind turbine (DFIG-WT) during the symmetrical and asymmetrical grid faults. Fault current limiter is economical and requires little maintenance during operation. They maintain rotor current and DC-link voltage to remain below the maximum acceptable limits during fault period. In this way they protect the back-back converters. Similar to a crowbar circuit, the fault current limiter circuitry also consists of diode bridge circuitry. In paper [23], [24] different works related to fault current limiter are presented.

2.3. Software based Approach:

These techniques under this class are mainly software-based control techniques, where different types of mathematical manipulations are done, in order to improve the performance. This includes virtual damping flux-based method, Impedance emulating method, PI control approach method etc.

These approaches are used to improve the control strategy of RSC and GSC to fulfil the FRT requirement. A robust controller is used in to improve the system transient response. Generally, a rotor reference current is calculated from the system parameters which is compared with the measured value of rotor current. Similarly, a reference grid filter current is calculated using parameter values and suitable mathematical expressions which is compared with measured value of grid current. After that, using appropriate control techniques, reference voltages of PWM converter are generated. Sometimes, only RSC is considered for control approach, and in that case, torque and reactive power is also used for proceeding with particular control approach. One of the very popular types of software-based control is virtual damping flux control.

Some examples of software-based approaches are:

2.3.1. Conventional PI controller-based approach:

It is the most primitive process of controlling a grid side and rotor side converter. In fact, there is nothing special in this method because the presence of this type of controller is inevitable in DFIG based wind turbines. The controller is designed by the use of vector control technique. They generally are associated with crowbars, in order to protect the rotor windings from overcurrent or other hardware devices.[25]

2.3.2 Virtual Damping flux-based approach:

During the fault condition, the transient flux causes a huge overshoot in rotor current. To suppress that, a virtual damping flux-based approach is undertaken in [26],[27]. In this method, we virtually calculate the amount of flux and then apply it in a separate loop to diminish the effect of it.

2.3.3. Feedforward Current Reference Approach:

At the time of significant grid fault, we need to inject transient and negative sequence component to the rotor current reference in order to obtain controllable Fault Ride through which cannot be addressed by classical PI controllers. In order to solve this, in this paper [28],

they discussed a feedforward current references control (FCRC) method for rotor side converter (RSC) to improve the fault ride through and system transient performance.

2.3.4. Inductance Emulating Control:

For doubly fed induction generator (DFIG)-based wind turbines, the rotor side converter is vulnerable to suffer from overcurrent during severe grid faults, due to large electromotive force (EMF) induced in the rotor circuit, resulting in a spike in dc link capacitor voltage and thus resulting in huge rotor overcurrent. To solve this problem, in this paper [29] an inductance-emulating control strategy for DFIG-based wind turbine is undertaken in order to suppress the huge rotor current in post fault period, thus improving its robustness and FRT capability. Under the proposed control strategy, once the grid fault is detected, the rotor side converter (RSC) is controlled to emulate a virtual inductance.

2.3.5. Sliding Mode Control based approach:

Sliding mode control is a nonlinear robust control methodology by which an error-based sliding surface is chosen. The objective of sliding mode control is to minimize the error between the reference and measured value to bring sliding surface=0 in finite time. Sliding surfaces are to be chosen such a way that Lyapunov criteria is satisfied. In paper [30], the DFIG grid fault has been minimized with the help of a sliding mode control-based methodology. We shall know more about sliding mode control in chapter 3. The disadvantage of this method is high frequency chattering effect which is harmful for power system circuitry. So, some advance manipulation can be done over this method to obtain better result. Our present work is accomplished with an advanced version of sliding mode control which we shall discuss later.

2.4. Flowchart of Different Fault ride Through Techniques:

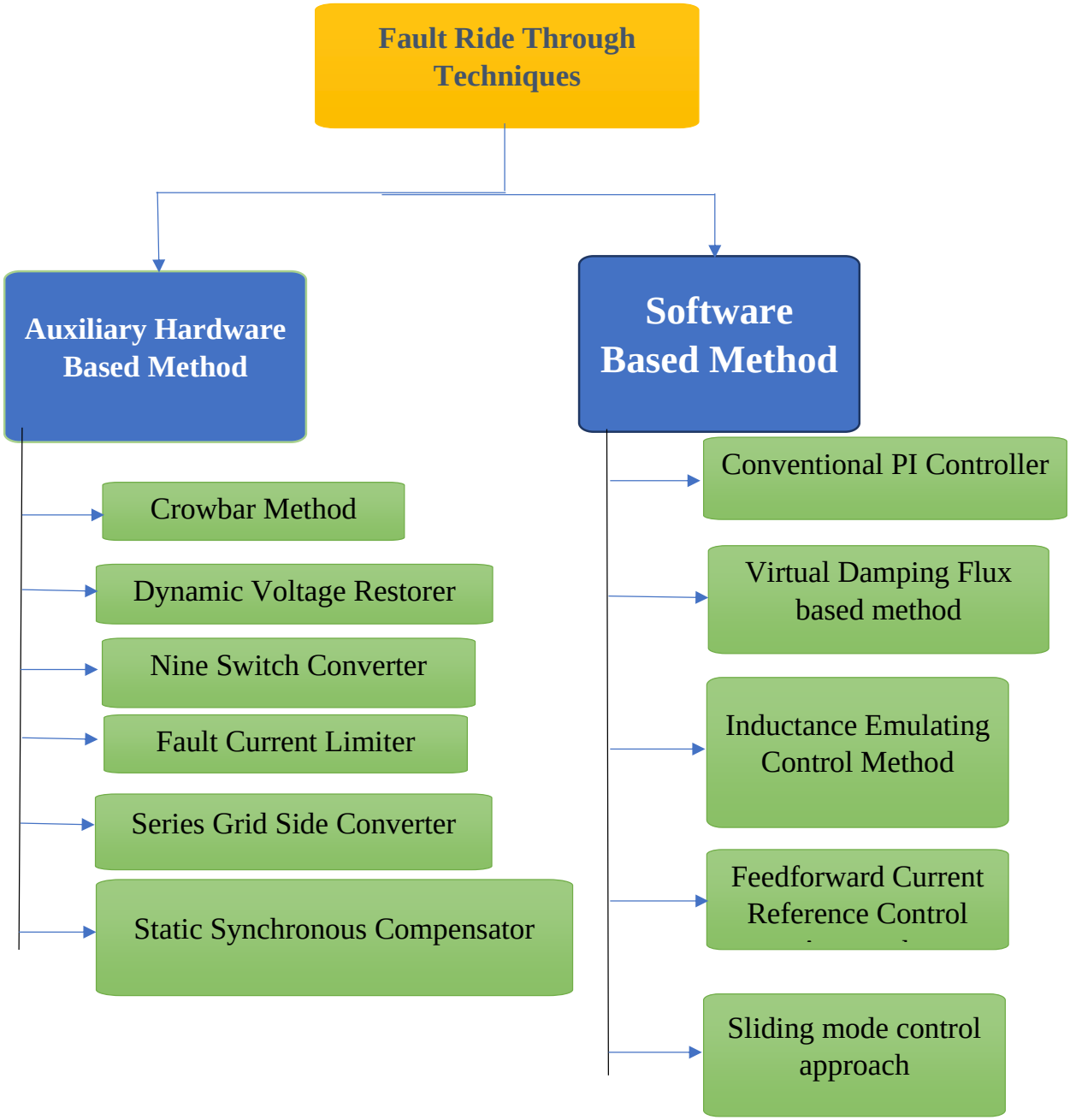

2.5. Chapter Summary:

In this chapter, we have discussed different types of hardware, software or hybrid type approaches that are undertaken previously in order to analyse fault ride through of DFIG. This discussion helps us to find out the advantage and disadvantage of the various techniques, also motivates us to apply newer mathematical or hardware-based techniques to improve the outputs furthermore.

Chapter 3

Introduction to Sliding Mode and Integral Terminal Sliding Mode Approach

3.1. Introduction:

In chapter 2, we already put some views over sliding mode control. Now for this particular thesis work, we have to introduce a newer type of Sliding mode control, that is integral terminal sliding mode control. As we know, a typical 1st order sliding mode control has several disadvantages, like chattering effect, so in order to overcome this, we are using a different approach, Integral Terminal Sliding mode control. It can be said as a part of Terminal Sliding mode control, where a terminal attractor in mathematical form is used in order to alleviate the chattering phenomenon and to ensure the finite time convergence. In subsequent sections and also in some parts of next chapter, we shall discuss about integral terminal Sliding mode control in more detail.

3.2. Revision of Sliding Mode Control:

Sliding Mode Control (**SMC**) is a nonlinear robust control method that alters the dynamics of a nonlinear system by applying a equivalent control signal along with a discontinuous control signal that drags the system to slide along a plane of the system's normal behaviour. Sliding mode control is a variable structure control method. The multiple control structures are designed so that system trajectories always move toward an adjacent region with a different control structure, and the ultimate trajectory will slide along the boundaries of the control structures. The motion of the system as it slides along these boundaries is called a sliding mode and the geometrical surface upon where the sliding takes place consisting of the boundaries is called sliding surface. [31]

3.2.1. Mathematical Approach of Sliding Mode Control:

Now let us focus into the mathematical approaches of sliding mode control. Considering a single input dynamic system:

$$x^{(n)} = f(x) + b(x)u \quad (1)$$

Where scalar x = output of interest

u = control input

$x^{(n)} = [x\ \dot{x}\ \dots\ \dots\ \dots\ x^{(n-1)}]^T$ = State Vector

Now according to the Sliding mode control, we have to build up an error surface which is known as Sliding surface. [32]

For that, let us denote

$$\check{x} = x_d - x, \text{ where } \check{x} = \text{Tracking error on variable x}$$

$$x_d = \text{Desired value of variable x}$$

To proceed with the sliding mode control, we have to design a time varying surface S(t) (Sliding Surface) which is:

$$S = \left(\frac{d}{dt} + \gamma\right)^{(n-1)} . \check{x} \quad (2)$$

Where, $\gamma = \text{Strictly positive Constant}$

n = Order of the System

3.2.2. Convergence Condition for Sliding Mode Control:

According to Lyapunov, the Stability of any nonlinear system is checked by taking a Lyapunov Candidate function (Which should be Positive definite in nature).

Where V is the Lyapunov Candidate function.

$$V = \frac{1}{2}S^2 \quad (3)$$

And, S is the Sliding surface.

Now, from the equation, it is clear that V is positive definite in nature. Now to satisfy the Lyapunov stability criterion, we have to check if, $\dot{V}$ or the derivative of positive definite function is lesser than 0 or not, i.e. we have to check if the derivative is negative definite or not. The asymptotic stability condition for the system is:

$$S\dot{S} \leq 0 \tag{4}$$

Or if the finite time convergence is to be given for a certain extent, then the equation would be:

$$\frac{1}{2}\frac{ds^2}{dt} \leq -\eta|s| \tag{5}$$

where η is a strictly positive constant. Unlike the previous equation, the addition of the value η ensures finite reaching time instead offering asymptotic stability.

Equation (5) states that the squared value of the distance to the surface, as measured by s^2, decreases along all system trajectories. Thus, it drags all the trajectories to the sliding surface as shown in the figure, making it an invariant set. That means once they are brought to the surface, they remain on the surface forever. This is the methodology of sliding mode control and this condition is called **sliding condition.**

S(t) verifying (5) is referred to as a sliding surface, and the system's behaviour once on the surface is called sliding regime or sliding manifold.

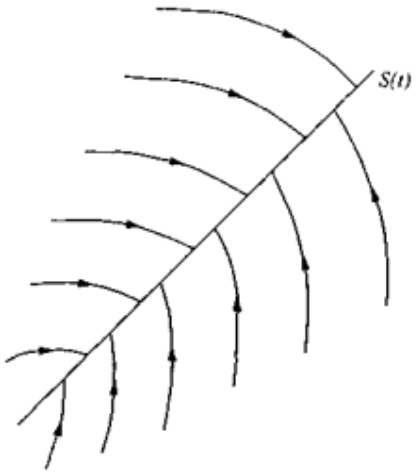

Figure 3.1. Sliding Condition [32]

Generally, it is based on the remark that it is much easier to control lst-order systems *(i.e.*, systems described by lst-order differential equations), be they nonlinear or uncertain, than it is to control systems described by higher order differential equations).

3.2.3. Equivalent Control law generation for Sliding Mode Control:

The system's motion on the sliding surface can be stated with an interesting geometric interpretation. The final condition of fulfilling the sliding mode control can be stated as a dynamic equation as follows:

$$\dot{S} = 0 \tag{6}$$

By these dynamics, we can state that when the rate of change of sliding surface is 0, it reaches to the sliding surface. Choosing Sliding surfaces wisely and performing all the mathematical manipulations for the control input, we can obtain expression for equivalent control for sliding mode control.

The control law for satisfying the above condition have 2 parts. In the first part we have to build an equivalent control according to the system dynamics. The second part is a discontinuous switching function that is known as switching or hitting control. This part basically consists of a signum function.

The control law can be expressed as:

$$U = U_{eq} + U^{hit} \tag{7}$$

Where,

$$U_{eq} = \text{Equivalent Control}$$

$$U^{hit} = \text{Switching or hitting control}$$

U^{hit} can be expressed by:

$$U^{hit} = -k\,\text{sign}(S(x,t)) \tag{8}$$

Here, k is controller gain, and sign function can mathematically be expressed by:

$$\begin{aligned} \text{sign}(S(x,t)) &= 1,\ S(x,t) > 0 \\ &= 0,\ S(x,t) = 0 \end{aligned} \tag{9}$$

$= -1, S(x,t) < 0$

The controller presents high robustness against parameter variations in uncertainty period, but as the convergence that depends on the hitting control or switching based on signum function is often imperfect (for instance, in practice switching is not instantaneous, and the value of s is not known with infinite precision), it leads to high-frequency switching (chattering phenomena) over the sliding surface due to the presence of discontinuous signum function involved. This is the main disadvantage of sliding mode control.

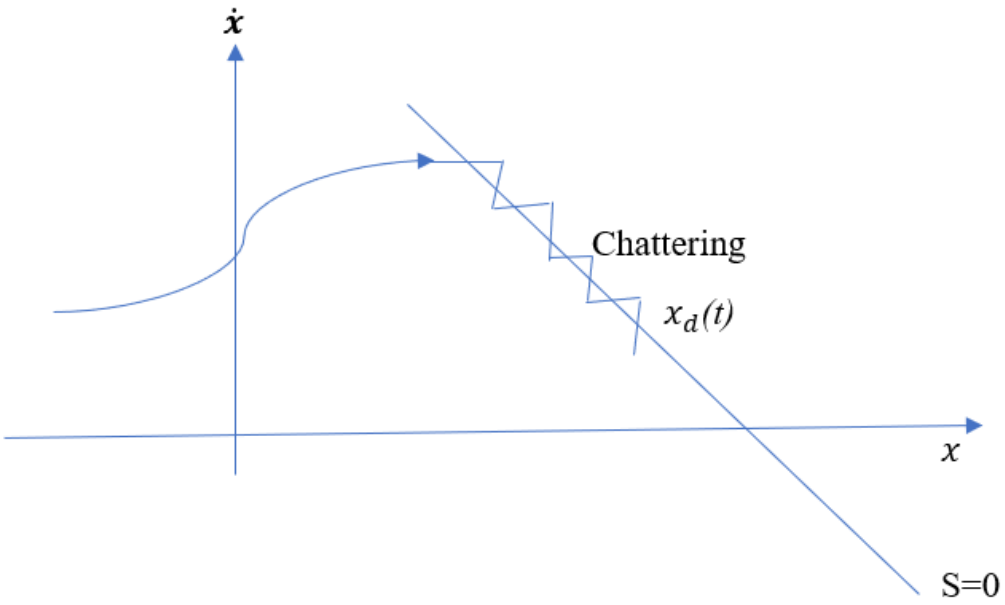

Figure 3.2: Sliding Surface and Chattering phenomenon [32]

3.3. Introduction to Terminal Sliding Mode Control:

In the early 1990s, an advanced version of sliding mode control named **Terminal sliding modes** (TSM) [33] was invented by Venkataraman and Gulati.[34] TSM is a mathematically manipulated version of conventional sliding mode control.

The main idea of terminal sliding mode control can be understood by the concept of terminal attractors which guarantee finite time convergence of the states. In conventional 1^{st} order type sliding mode control, the convergence condition is guaranteed in terms of asymptotic stability. Means the system will reach to its stable position, but in infinite time. In TSM, the sliding surface or sliding manifold is taken such a way that some nonlinear terms are used in its equation and the manifold acts as a terminal attractor, that drags the system response to its convergence in a finite time. [33]

There are some variations of the TSM including: Non-singular TSM(NTSM)[33], Fast TSM(FTSM)[33], Integral Terminal Sliding mode control (ITSMC)[33] etc. Terminal sliding mode is also applied in different applications of nonlinear process control, for example, rigid robot manipulators control etc. It is worth to be mentioned that the approach of TSMC is non-Lipschitz.

The concept of Terminal Sliding Mode (TSM) is based on a notion of terminal attractors [37] for studying the content addressable memory in neural networks. The first specific use in control design was in [38] where the following basic TSM form was used for controlling the second-order systems.

Although it can alleviate the drawbacks of conventional sliding mode control to some extent, still it has some disadvantages such as singularity problem. To further alleviate this problem, we introduce an integral terminal sliding mode control that is to be discussed in detail.

3.4. Integral Terminal Sliding Mode Control:

The approach here presented as 'Integral Sliding control design' directly uses the TSM/FTSM/NTSM as the reaching law and the sliding mode is of the same dimension of the system to be controlled. All of these methods are called the integral TSMC (ITSMC). Integral Terminal sliding mode control is a class of Terminal sliding mode control which focuses on reducing the singularity problem and ensure fast finite time convergence. This would result in somehow a control without discontinuous though robustness features may be compromised. In

[39], an ITSMC approach was discussed for output tracking of a nonlinear MIMO system of relative degree 1.

In [39], the derivative-integral TSMC technique was used to suppress the chaotic behaviours in complex and uncertain biological systems. The model simulation results clearly indicated that the settling time using the derivative-integral TSMC technique is around 22% of that using the first and high-order SMC technique, and the state errors using the derivative-integral TSMC technique is nearly 5% while comparing with the first and high-order SMC techniques.

3.4.1. Mathematical Formulation of Integral Terminal Sliding mode control in nonlinear system:

The ITSMC method is presented to achieve the control objective $\lim_{t\to\infty} y(t) - y_d(t)$ for relative-degree-one systems with all $r_i = 1$. Here, the tracking error is defined as $e(t) = y(t) - y_d(t)$. Instead of using a linear sliding function, a novel nonlinear sliding function- sign function based integral terminal sliding mode control is discussed. [39]

- **Sign integral terminal sliding mode control:**

For relative-degree-one systems the sign integral terminal sliding function is taken as follows:

$$s(t) = e(t) + \alpha e_I(t) \tag{10}$$

$$\dot{e}_I(t) = \text{sign}(e(t)), \quad \text{with } e_I(0) = -e(0)/\alpha \tag{11}$$

where $\alpha > 0$ and $e_I(t)$ is the integration of sign(e(t)) and has the initial value $-e(0)/\alpha$, and $\text{sign}(e) \equiv [\text{sign}(e_1) \cdots \text{sign}(e_m)]^T$ for e_I $(n = 1, \ldots, m)$ is the n-th element of the error vector e. In other words, the sign integral terminal sliding function can be rewritten in the following form:

$$s(t) = e(t) + \alpha \int_0^t \text{sign}(e(\tau))d\tau \text{ , and } s(0) = 0 \tag{12}$$

If the sliding surface s(t) is always kept at zero such that $e(t) = -\alpha e_I(t)$, then the derivative of sign integration (11) becomes $\dot{e}_I(t) = -\text{sign}(\alpha e_I(t))$. Then, $e_I(t)$ will converge to zero in the finite time.

$$T_s = |e_I(0)| = \frac{|e(0)|}{\alpha} \quad (13)$$

The convergence of the tracking error $e(t)$ is occurred in the same finite time because the error equation $e(t) = -\alpha e_I(t)$ remains on the surface $s(t) = 0$.

The system is forced to start on the TSM, and the final reaching phase is eliminated. Therefore, the singular problem is avoided due to the utilization of the ITSM.

Consider the following the Lyapunov function:

$$V_L = \frac{1}{2} S^T S$$

To guarantee its convergence, we must ensure that its derivative is negative.

$$\dot{V}_L = S^T \dot{S}$$

The rest procedure is similar with sliding mode control or any other nonlinear control techniques.

3.5. Chapter Summary:

In this chapter, the theoretical approaches that are to be undertaken for the thesis work has been discussed. The basics of Conventional first order sliding mode control and equivalent control laws are generated here. Also, the basics of Integral Terminal sliding Mode Control, the finite time convergence time is also presented.

Chapter 4

Mathematical Derivation for Grid Connected DFIG based WECS System

4.1. Introduction:

In this chapter we shall discuss about mathematical formulation that is required for our simulation. As discussed in chapter 2, we shall start with the mathematical modelling of DFIG. This will give us the set of equations that we can use to create our sliding surfaces. After that, using the mathematical equations, we shall try to form sliding surfaces that will be useful in thesis work.

4.2. Mathematical Modelling of wind turbine:

The mechanical power generated by the wind turbine is:

$$P = 0.5A\rho C_p V_w^3 \quad (14)$$

Where, *P* is the power in W, ρ the air density in g/m^3, C_p is a dimensionless factor called power coefficient, *A* the turbine rotor area in m^2 and V_w is the wind speed in m/s. [40]

Ideally, power coefficient *Cp* maximum value equal to *Cp* = 0.593 [41] which means that the maximum power extracted from the wind cannot be more than 59.3% (Betz 's limit), because various mechanical and aerodynamic losses occur due to rotor construction (Shape of blades, weight, stiffness, etc.) which eventually degrades the amount of useful power from wind turbine. The power coefficient can be utilized in the form of a function. The general function defining the power coefficient as a function of the tip-speed ratio and the pitch angle is defined as [42]

$$c_p(\lambda, \theta) = c_1 \left(c_2 \cdot \frac{1}{\beta} - c_3 \theta - c_4 \theta^x - c_5 \right) e^{-c_6 \frac{1}{\beta}} \quad (15)$$

The standard values of the coefficients c_1, = 0.5, c_2 = 116, c_3 = 0.4, c_4 , = 0, c_5 = 5, c_6 = 0.068. The parameter β can be expressed with the following equation:

$$\frac{1}{\beta} = \frac{1}{\lambda+0.08\theta} - \frac{0.035}{1+\theta^3} \quad (16)$$

Where θ is the pitch angle, which is the angle between the plane of rotation and the blade cross-sectional area. Now and the tip-speed ratio is defined as:

$$\lambda = \frac{RW_w}{V_w} \quad (17)$$

Where, R= radius of wind turbine blade.

The amount of aerodynamic torque (T_w) in Nm is given by the ratio between the harnessed power of wind turbine (Pw) and the turbine rotor speed in rad/s, as follows:

$$T_w = \frac{P_w}{W_w} \quad (18)$$

If the gearbox ratio of the machine is n_g the mechanical torque transmitted to the generator (T_m) in terms of aerodynamic torque will be:

$$T_m = \frac{T_w}{n_g} \quad (19)$$

4.3. Mathematical modelling of DFIG:

The mathematical modelling of DFIG is done by synchronously rotating dq axis modelling. Making it into rotating reference frame, it is easier to analyse the system. In high power (Megawatt range) Wind turbines, DFIG is the most widely used electrical generator [43].

4.3.1. Mathematical Modelling of DFIG Stator and Rotor:

The vector control of the DFIG is performed with the help of synchronously rotating dq reference frame. The stator flux vector position is oriented along the direct-axis [44], [45]. The implementation of the control of the rotor side converter the stator and rotor currents along with the stator voltage and rotor position is required to be known. [33] The stator flux-based orientation helps to make the torque expression only dependent upon the q axis component of rotor current. The below figure represents the d and q axis circuit diagram respectively of DFIG machine. By applying KVL, we can find the rotor voltage equations in synchronously rotating frame.

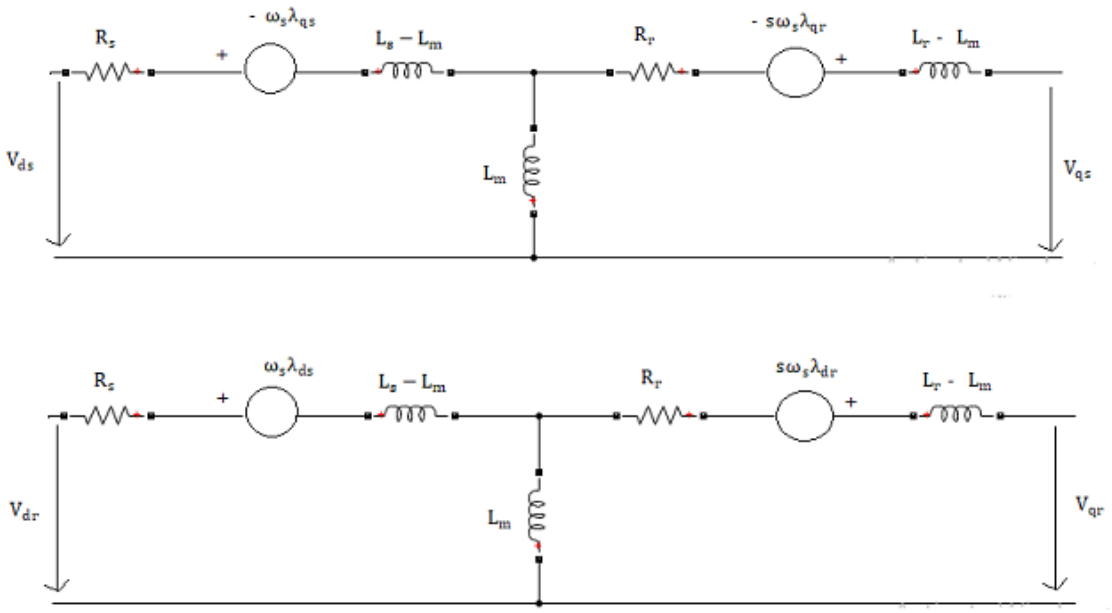

Figure 4.1. dq axis circuit diagram of Doubly fed Induction generator [46]

From the figure, the voltage equations can be derived as follows:

$$V_{ds} = R_s I_{ds} + \frac{d\lambda_{ds}}{dt} - w_s\lambda_{qs} \quad (20)$$

$$V_{qs} = R_s I_{qs} + \frac{d\lambda_{qs}}{dt} + w_s\lambda_{ds} \quad (21)$$

$$V_{dr} = R_r I_{dr} + \frac{d\lambda_{dr}}{dt} - (w_s - w_r)\lambda_{dr} \quad (22)$$

$$V_{qr} = R_r I_{qr} + \frac{d\lambda_{qr}}{dt} - (w_s - w_r)\lambda_{qr} \quad (23)$$

After obtaining the stator and rotor dq axis voltage expression, next our target is to calculate the stator and rotor dq axis flux linkages. They are given in the following equations:

$$\lambda_{ds} = L_s I_{ds} + L_m I_{dr} \quad (24)$$

$$\lambda_{qs} = L_s I_{qs} + L_m I_{qr} \quad (25)$$

$$\lambda_{dr} = L_r I_{dr} + L_m I_{ds} \quad (26)$$

$$\lambda_{qr} = L_r I_{qr} + L_m I_{qs} \quad (27)$$

Next our target is to calculate the stator active and reactive powers. Considering the d axis components as real and q axis components as imaginary, we can solve easily the equations for active and reactive power as follows:

$$P_s = 3/2 (V_{ds}I_{ds} + V_{qs}I_{qs}) \quad (28)$$

$$Q_s = 3/2(V_{qs}I_{ds} - V_{ds}I_{qs}) \quad (29)$$

Similarly, the rotor active and reactive power can be deduced as:

$$P_r = 3/2 (V_{dr}I_{dr} + V_{qr}I_{qr}) \quad (30)$$

$$Q_r = 3/2(V_{qr}I_{dr} - V_{dr}I_{qr}) \quad (31)$$

And the electromagnetic torque equation is given by:

$$T_e = \frac{3p}{4} \frac{L_m}{L_s} (\lambda_{qs}I_{dr} - \lambda_{ds}I_{qr})$$

$$\text{Or,} \quad T_e = \frac{3p}{4} L_m (I_{qs}I_{dr} - I_{ds}I_{qr}) \quad (32)$$

$$[\text{Because, } \frac{\lambda_{qs}}{L_s} = I_{qs} \text{ and } \frac{\lambda_{ds}}{L_s} = I_{ds}]$$

where p is the pole number.

4.3.2. Mathematical Modelling of Back-to-Back PWM Converter:

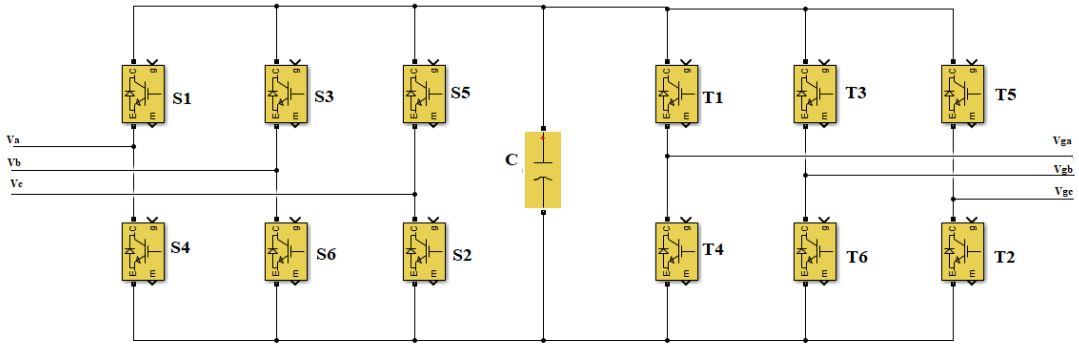

Figure 4.2. Schematic of back-to-back converter [47]

RSC and GSC are assumed to be as two controllable voltage source converters. For the sake of developing the dq axis voltage equations, here we have to design the stator voltage space vector along the q-axis. The reference frames for DFIG model, RSC and GSC control are all aligned with the stator voltage. The RSC and GSC voltages are generated through the afore-mentioned control blocks. In MATLAB/SIMULINK, feedback control blocks can be built. The converter controls can then be integrated with the DFIG model in the same dq reference frame.

There is one relationship that is to be discussed: the DC-link capacitor dynamics or the relationship between the RSC and the GSC. The DC-link capacitor dynamics has to be considered as well. So, now we shall discuss about Grid Side topology.

Grid Side Converter:

The objective of grid side converter control is to maintain the DC link voltage constant. For this a suitable PI controller is used with proper tuning of gain. Direct axis current can be obtained using the controller by comparing measured and reference value of DC link voltage, and quadrature axis current component can be obtained to by calculating the reactive power flow between the grid side converter and the grid. Here the grid voltage is aligned with the d axis reference frame. As we know, the rms voltage value of the microgrid system is constant, the grid voltage V_g can be expressed as V_{dg}.

$$V_{dg} = V_g$$

$$V_{qg} = 0 \qquad (33)$$

Active Power injected to the grid can be stated as:

$$P_g = 3/2\ (V_{dg}I_{df} + V_{qg}I_{qf})$$

Or, $$P_g = 1.5V_{dg}I_{df} \quad (34)$$

Reactive Power injected to the grid can be given as:

$$Q_g = 3/2(V_{qg}I_{df} - V_{dg}I_{qf})$$

Or, $$Q_g = -1.5V_{dg}I_{qf} \quad (35)$$

In a typical grid filter model, the voltage equation can be written as follows:

$$V_g = -(R_f + j\omega L_f)I_f - L_f\frac{dI_f}{dt} + V_f \quad (36)$$

where I_f is grid-filter current flowing through RL grid filter and V_f is the grid side converter output voltage.

Hence the dq axis voltages of GSC output can be expressed as follows:

$$V_{df} = R_fI_{df} + L_f\frac{dI_{df}}{dt} - w_sL_fI_{qf} + V_{dg} \quad (37)$$

$$V_{qf} = R_fI_{qf} + L_f\frac{dI_{qf}}{dt} - w_sL_fI_{df} + V_{qg} \quad (38)$$

Here V_{df}, V_{qf} are the dq axis voltages at the output end of GSC converter and I_{df}, I_{qf} are the dq axis currents that are flowing to the grid through the grid RL filter.

Similar like rotor side converter, the decoupled power flow control between the GSC and the grid will be proportional to I_{df} and I_{qf}. The energy stored by the DC-link capacitor is expressed as follows:

$$\frac{dW}{dt} = 0.5\ C\frac{dV_{dc}^2}{dt} = -P_g - P_r \quad (39)$$

4.4. Clarke and Park Transformation:

The Clarke transformation transforms the 3-phase system a,b,c to the two orthogonal coordinate system (α,β). This transformation transforms the three-phase reference frame to the two-phase stationary reference frame.

The Park Transformation transforms the 3 phase a,b,c co-ordinate into a synchronously rotating dq0 reference frame. To perform this, one more parameter is needed which is the angular position ωt.

When the rotating frame alignment at ωt=0 is 90 degrees behind the phase A axis, a positive-sequence signal with Mag=1 and Phase=0 degrees yield the following dq values: d=1, q=0.

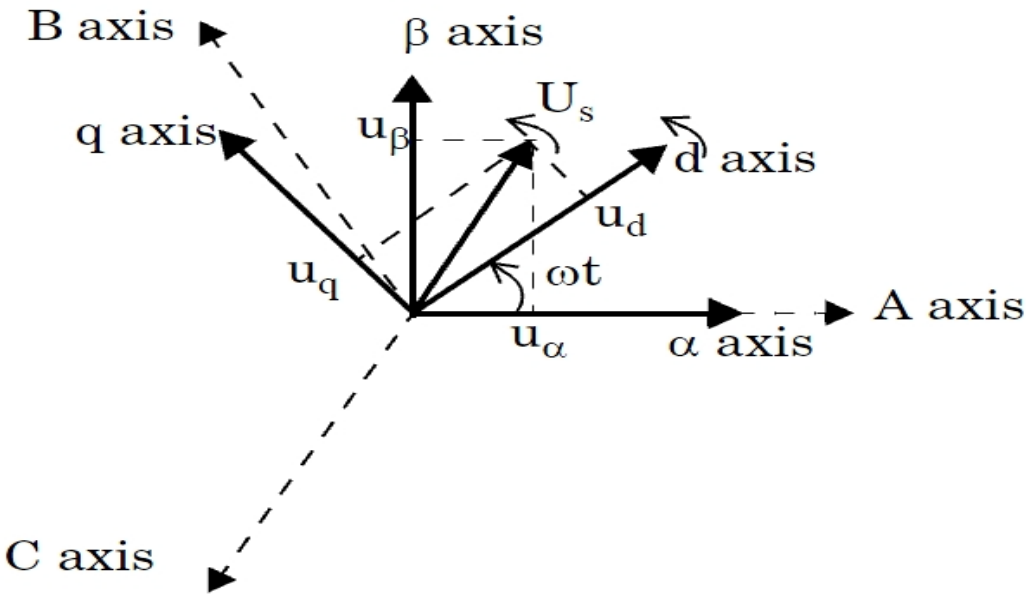

Figure 4.3. Phasor diagram of dq to abc conversion [48]

4.5. Angle Estimation [49]:

For the estimation of the rotor angle and the grid angle we use PLL block available in MATLAB/SIMULINK. However, the mathematical calculation of figuring out the angles are shown below:

$$\theta_s = \tan^{-1}\frac{v_{qs}}{v_{ds}} \quad (40)$$

$$\theta_r = \theta_s - \frac{\pi}{2} - \theta_e \quad (41)$$

$$\theta_e = p\theta_m \quad (42)$$

Where,

θ_s is the stator angle

θ_r is the rotor angle

θ_e is the electrical angle

The stator is directly connected to the grid so that the grid angle is equivalent to the stator angle. The rotor angle can be estimated from the stator angle using above formulae**.** The grid is synchronised using a PLL block.

4.6. Control Implementation using conventional PI control:

To implement PI based control of DFIG machine, vector control approach is most widely used. The vector control of the induction machine is performed by the current control loops. The It is a very nice approach to address limited speed range electrical drive systems [50]. The use of the suitable power converter in the rotor side, the overall system control can be performed with low current harmonic distortion in both stator and rotor side [45], [50]. The space vector theory is used to express the three-phase quantities in terms of the space vectors. Vector control modelling describes induction machine describes its transient and steady state performance. [51]. The three phase quantities are converted to synchronously rotating frame in order to address the system dynamics in a convenient way.[52]. The system becomes simpler and

simplifies the understanding of the control process. In the work, we specifically use stator flux-oriented vector control.

We previously mentioned that the vector control here is done based on stator flux-oriented control. In order to obtain better control, we align stator flux along d axis [30]. That results in:

$$\lambda_{ds} = \lambda_s \text{ and } \lambda_{qs} = 0$$

Putting the values in equation (20) and (21)

$$V_{ds} = R_s I_{ds} + \frac{d\lambda_{ds}}{dt} \quad (43)$$

$$V_{qs} = R_s I_{qs} + w_s \lambda_s \quad (44)$$

Assuming λ_{ds} to be constant in steady state, and stable electrical network, we can take the constant stator flux in the system, which means derivative term of λ_{ds} is also zero. So the new voltage equation will be:

$$V_{ds} = R_s I_{ds} \quad (45)$$

$$V_{qs} = R_s I_{qs} + w_s \lambda_s \quad (46)$$

Putting the values of λ_{ds} *and* λ_{qs} to the equation (24) and (25) we can obtain:

$$I_{qs} = -\frac{L_m}{L_s} I_{qr} \quad (47)$$

$$I_{ds} = -\frac{L_m}{L_s} I_{dr} + \frac{\lambda_s}{L_s} \quad (48)$$

$$T_e = -\frac{3p}{4}\frac{L_m}{L_s}\lambda_s I_{qr} \quad (49)$$

Substituting the equations (45),(46) and (47) to the equation (30) and (31) :

$$P_s = \frac{3}{2}\left(\frac{w_s L_m \lambda_s I_{qr}}{L_s} - \frac{\left(V_s^2 - w_s^2 \lambda_s^2\right)}{R_s}\right) \quad (50)$$

$$Q_s = \frac{3}{2}\left(\frac{w_s L_m \lambda_s I_{qr}}{L_s} - \frac{\left(w_s \lambda_s^2\right)}{R_s}\right) \quad (51)$$

4.6.1. Rotor Side Converter Control Implementation:

The vector control of the DFIG is performed in the synchronously rotating dq reference frame. The stator flux vector position is oriented along the direct-axis [44], [45]. The implementation of the control of the rotor side converter the stator and rotor currents along with the stator voltage and rotor position is required to be known. The advantage of the stator flux orientation is that the torque is only dependent on the quadrature axis component of the rotor current [33]. The equations obtained for the rotor voltage in synchronous reference frame as the function of the rotor currents is as shown below:

By analysing the equations (50) and (51), we can see that a decoupled power control can easily be done; where the component I_{qr} of the rotor current is directly related to active power, so it can control active power. Similarly, the reactive power can be controlled by I_{dr}. By rearranging equations (22) and (23) we can deduce a formula of rotor currents as a function of rotor voltages.

$$V_{dr} = R_r I_{dr} + \sigma L_r \frac{di_{qr}}{dt} - \sigma w_r L_r i_{qr} + w_r \frac{L_m}{L_s} \frac{d\lambda_s}{dt} \quad (52)$$

$$V_{qr} = R_r I_{qr} + \sigma L_r \frac{di_{dr}}{dt} - \sigma w_r L_r i_{dr} + w_r \frac{L_m}{L_s} \frac{d\lambda_s}{dt} \quad (53)$$

Where,

$$\sigma = 1 - \frac{L_m{}^2}{L_s L_r} \quad (54)$$

The stator flux is constant since the grid is connected to the stator of the DFIG, this implies that the derivative term$\left|\frac{d\lambda_s}{dt}\right.$ is zero. For the transformation in the reference frame, the angle θr has to be estimated. The block diagram for the rotor side converter control of the induction machine is provided below form reference.

The block diagram for close loop current control of rotor side converter is shown below:

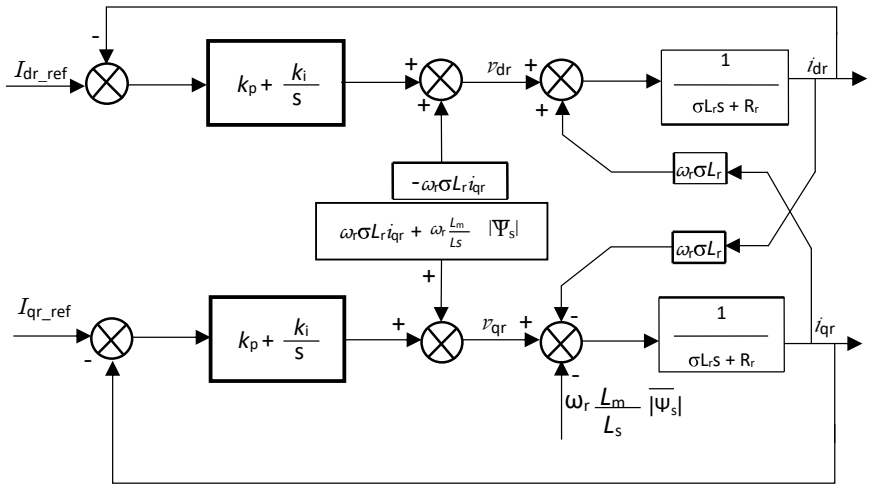

Figure 4.4. Current control loop of Rotor side converter with Conventional PI control [53]

The transfer function for dq axis current loop modelling can be expressed using the block diagram as follows:

$$\frac{i_{dr}}{i_{dr\_ref}} = \frac{sK_p + K_i}{L_f s^2 \sigma + s(K_p + R_r) + K_i} \tag{55}$$

$$\frac{i_{qr}}{i_{qr\_ref}} = \frac{sK_p + K_i}{L_f s^2 \sigma + s(K_p + R_r) + K_i} \tag{56}$$

When the denominators of the above 2 transfer functions are compared with the denominator of general second order control transfer function i.e., $s^2 + 2\xi\omega_n s + \omega_n{}^2$ we have,

$$K_i = L_r \omega_n{}^2 \sigma \tag{57}$$

$$K_p = 2\sigma L_r \xi \omega_n{}^2 - R_r \tag{58}$$

The above-mentioned values are proportional and the integral gain constant for the PI-controller in the rotor side converter control.

4.6.2. Grid Side Converter Control Implementation:

The grid side converter is fed from the grid using the RL-filter. Taking the Laplace transformation in the voltage equations of the grid side converter yields the following transfer function:

$$\frac{i_{df}}{V_{dg}} = \frac{1}{L_f s + R_f} \tag{59}$$

$$\frac{i_{qf}}{V_{qg}} = \frac{1}{L_f s + R_f} \tag{60}$$

The block diagram for the grid side converter control loop is shown in the figure below**:**

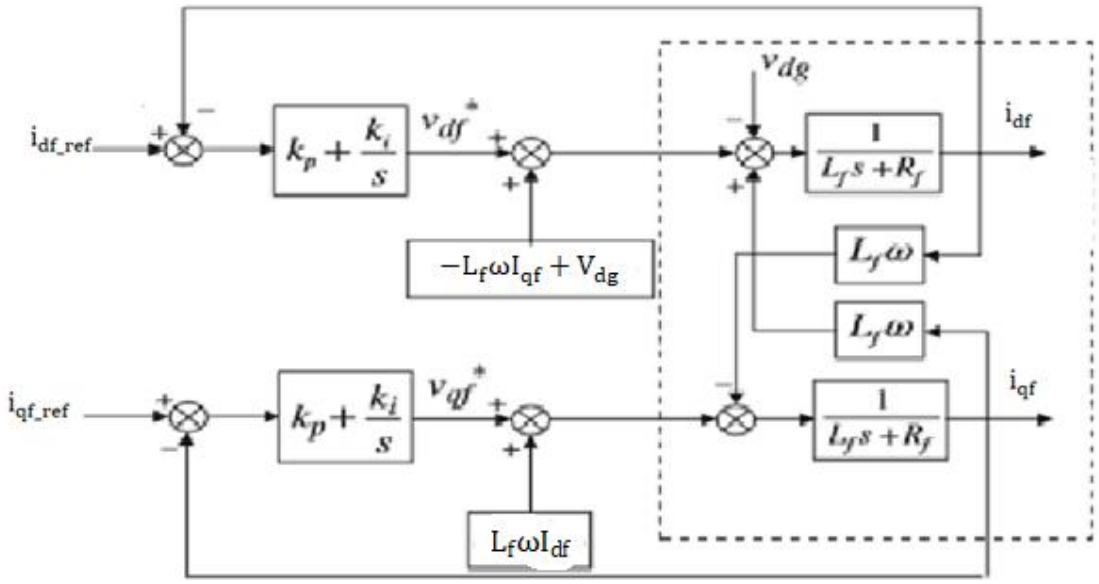

Figure 4.5. Current control loop of Grid side converter with Conventional PI control [53]

The transfer function for dq axis current loop modelling can be expressed using the block diagram as follows:

$$\frac{i_{df}}{i_{df\_ref}} = \frac{sK_p + K_i}{L_f s^2 + s(K_p + R_f) + K_i} \tag{61}$$

$$\frac{i_{qf}}{i_{qf\_ref}} = \frac{sK_p + K_i}{L_f s^2 + s(K_p + R_f) + K_i} \quad (62)$$

When the denominators of the above 2 transfer functions are compared with the denominator of general second order control transfer function i.e., $s^2 + 2\xi\omega_n s + {\omega_n}^2$, we have:

$$K_i = L_f {\omega_n}^2 \quad (63)$$

$$K_p = 2L_f \xi {\omega_n}^2 - R_f \quad (64)$$

The above-mentioned values are proportional and the integral gain constant for the PI-controller in the rotor side converter control.

In the block diagram, PLL is used to estimate the grid angle while in this thesis the grid angle is calculated using angle calculation block which will explained in the later section.

The constant gains in the above block diagram are defined as below:

$$K_{pg} = \frac{1}{\frac{3}{2}V_{dg}}$$

$$K_{qg} = -\frac{1}{\frac{3}{2}V_{dg}} \quad (65)$$

4.7. Control Implementation using sliding mode control:

The theory for sliding mode control is already discussed in chapter 3. Now we shall implement it in the DFIG system to generate control law (Reference voltage) for RSC and GSC respectively.

4.7.1. Rotor Side Converter Control:

Rearranging equation (52) and (53),

$$\frac{dI_{qr}}{dt} = \frac{1}{\sigma L_r}\left(V_{qr} - R_r I_{dr} - sV_{qr}\sigma I_{dr} - \frac{sw_s L_m \lambda_s}{L_s}\right) \quad (66)$$

$$\frac{dI_{dr}}{dt} = \frac{1}{\sigma L_r}\left(V_{qr} - R_r I_{qr} + sV_{dr}\sigma I_{qr}\right) \quad (67)$$

Now, for designing the Rotor Side Converter Control, we need to declare the sliding surfaces. As our main focus is kept on the uncertainty of rotor d and q axis currents, the sliding error surfaces are based on the difference between reference and measured value of dq axis rotor currents.

So, the Sliding Surfaces are taken as:

$$s_d(I_{dr}) = I_{dr\_ref} - I_{dr} \tag{68}$$

$$s_d(I_{qr}) = I_{qr\_ref} - I_{qr} \tag{69}$$

The derivatives of the sliding surfaces are given by:

$$\dot{s}_d(I_{dr}) = \dot{I}_{dr\_ref} - \dot{I}_{dr} \tag{70}$$

$$\dot{s}_q(I_{qr}) = \dot{I}_{qr\_ref} - \dot{I}_{qr} \tag{71}$$

From the above two equations, the d axis sliding mode invariance condition can be stated as:

$$s_d(I_{dr}) = \left(I_{dr_{ref}} - I_{dr}\right) = 0$$
$$\dot{s}_d(I_{dr}) = 0 \tag{72}$$

Now the final objective of this control method is to generate reference voltage signals for VSC type Rotor side converter. So, the control law will be in terms of Rotor dq axis voltages. According to the sliding mode control, the d axis voltage control law can be expressed as follows:

$$V_{dr} = V_{dr}^{eq} + V_{dr}^{hit} \tag{73}$$

Here, $V_{dr}^{eq} = \text{d axis Equivalent Control}$

$V_{dr}^{hit} = \text{d axis Switching or hitting Control}$

So, by from the equation (52) and equation (22), we can get:

$$V_{dr}^{eq} = -\frac{2}{3}\frac{\sigma L_r L_s}{w_s L_m \lambda_s}\dot{Q}_{s_{ref}} + R_r I_{dr} - s w_s \sigma L_r I_{qr} + \frac{\sigma L_r \lambda_s}{L_m} \tag{74}$$

Where, $$I_{dr\_ref} = -\frac{2}{3}\frac{L_s}{w_s L_m \lambda_s}\left(Q_{s_{ref}} - \frac{3}{2}\frac{w_s \lambda_s^2}{L_s}\right) \tag{75}$$

Similarly, the q axis sliding mode invariance condition can be stated as:

$$s_q(I_{qr}) = (I_{qr_{ref}} - I_{qr}) = 0$$
$$\dot{s}_q(I_{qr}) = 0 \tag{76}$$

Similarly, the q axis voltage control law can be expressed as follows:

$$V_{qr} = V_{qr}^{eq} + V_{qr}^{hit} \tag{77}$$

So, by putting the equation (51) to equation (23), we can get

$$V_{qr}^{eq} = \frac{2}{3}\frac{\sigma L_r L_s}{w_s L_m \lambda_s}\dot{P}_{s_{ref}} + R_r I_{qr} + sV_{qr}\sigma I_{dr} + \frac{sw_s L_m \lambda_s}{L_s} + L_s\frac{(V_s^2 - w_s^2\lambda_s^2)}{w_s L_m \lambda_s R_s} \tag{78}$$

$$\text{Where, } I_{qr_{ref}} = \frac{L_s}{w_s L_m \lambda_s}\left(\frac{2P_{s_{ref}}}{3} + \frac{(V_s^2 - w_s^2\lambda_s^2)}{w_s L_m \lambda_s R_s}\right) \tag{79}$$

The control law thus can be set by:

$$V_{dr} = V_{dr}^{eq} - k_d \text{sign}(s_d)$$
$$V_{qr} = V_{qr}^{eq} - k_q \text{sign}(s_q) \tag{80}$$

Where k_d and k_q are switching gains>0.

The generated reference voltages are converter from dq to abc coordinate, and after that they are fed to the PWM converter.

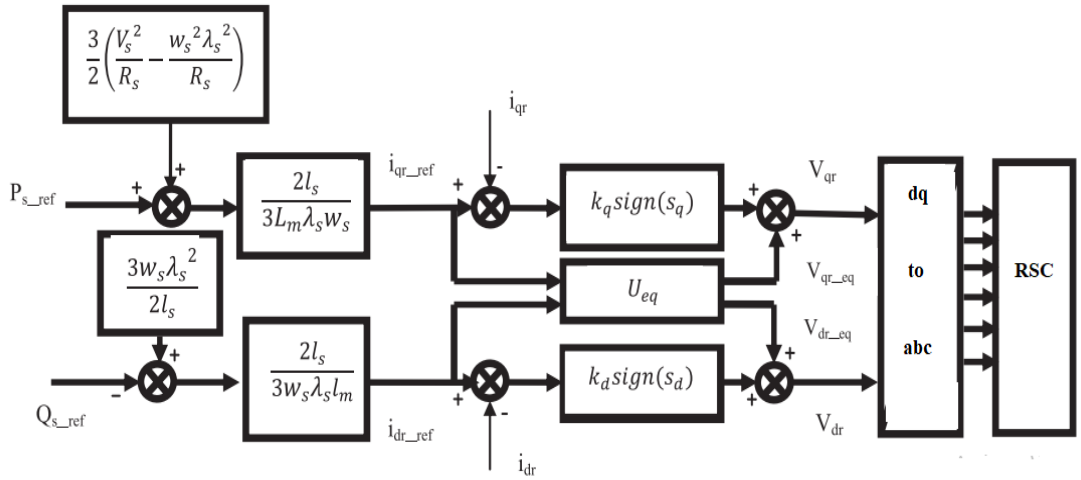

Figure 4.6: Control Implementation of Grid Side Converter with SMC approach [30]

4.7.2. Grid Side Converter Control Implementation:

Now, for designing the Grid Side Converter Control, we need to declare the sliding surfaces. As our main focus is kept on the uncertainty of grid filter d and q axis currents, the sliding error surfaces are based on the difference between reference and measured value of dq axis grid filter currents.

Rearranging the equations (37) and (38) we get:

$$\frac{dI_{df}}{dt} = \frac{1}{L_f}(V_{df} - R_f I_{df} + w_s L_f I_{qf} - V_{dg}) \quad (81)$$

$$\frac{dI_{qf}}{dt} = \frac{1}{L_f}(V_{qf} - R_f I_{qf} + w_s L_f I_{df} - V_{qg}) \quad (82)$$

So, the Sliding Surfaces are taken as:

$$s_1(I_{df}) = I_{df\_ref} - I_{df} \quad (83)$$

$$s_2(I_{qf}) = I_{qf\_ref} - I_{qf} \quad (84)$$

The derivative of the sliding surfaces are given by:

$$\dot{s}_1(I_{df}) = \dot{I}_{df\_ref} - \dot{I}_{df} \quad (85)$$

$$\dot{s}_2(I_{qf}) = \dot{I}_{qf\_ref} - \dot{I}_{qf} \quad (86)$$

From the above two equations, the d axis sliding mode invariance condition can be stated as:

$$s_1(I_{df}) = (I_{df\_ref} - I_{df}) = 0$$

$$\dot{s}_1(I_{df}) = 0 \quad (87)$$

Now the final objective of this control method is to generate reference voltage signals for VSC type Rotor side converter. So, the control law will be in terms of Rotor dq axis voltages. According to the sliding mode control, the d axis voltage control law can be expressed as follows:

$$V_{df} = V_{df}^{eq} + V_{df}^{hit} \quad (88)$$

Here, $V_{df}^{eq} = \text{d axis Equivalent Control}$

$V_{df}^{hit} = \text{d axis Switching or hitting Control}$

So, by rearranging the equations we can get:

$$V_{dg}^{eq} = \left(\frac{2}{3}\frac{\sigma L_f}{V_{dg}}\dot{P}_{s\_ref} + R_f I_{df} + w_s L_f I_{qf} - V_{dg}\right) \quad (89)$$

Similarly, the q axis sliding mode invariance condition can be stated as:

$$s_2(I_{qf}) = (I_{qf\_ref} - I_{qf}) = 0$$

$$\dot{s}_2(I_{qf}) = 0 \quad (90)$$

Designing the control law:

$$V_{qf} = V_{qf}^{eq} + V_{qf}^{hit} \quad (91)$$

Here, $V_{qf}^{eq} = \text{q axis Equivalent Control}$

$V_{qf}^{hit} = \text{q axis Switching or hitting Control}$

So, from the equation of q axis voltage, we can get:

$$V_{qf}^{eq} = -\frac{2}{3}\frac{\sigma L_f}{V_{dg}}\dot{Q}_{s\_ref} + R_f I_{qf} + w_s L_f I_{df} \quad (92)$$

To obtain good dynamic performance, the control vector is imposed as follows:

$$V_{df} = V_{df}^{eq} - k_{gd}\,\mathrm{sign}(s_1)$$

$$V_{qf} = V_{qf}^{eq} - k_{gq}\,\mathrm{sign}(s_2) \quad (93)$$

Where k_{gd} and k_{gq} are switching gains>0

This is the control law generated for the grid side converter. The d and q axis reference voltages are used to generate pulses with the help of a PWM converter.

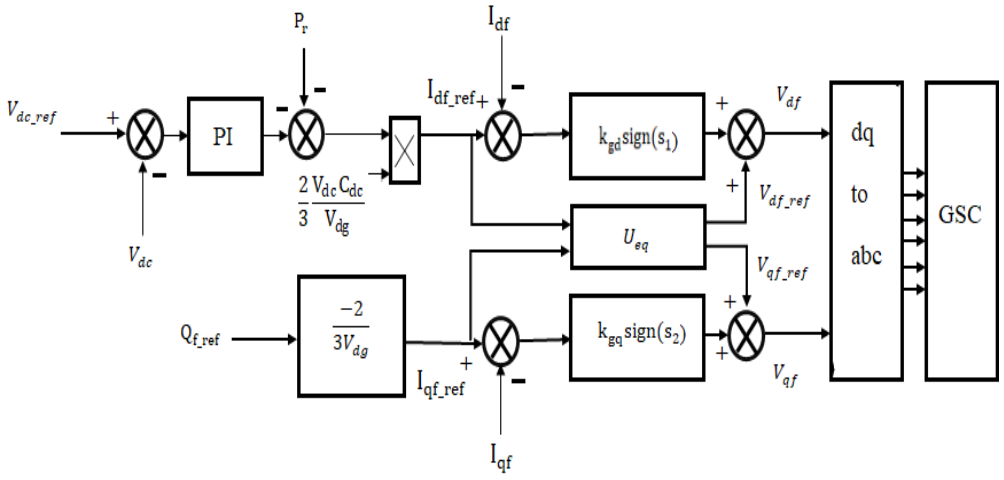

Figure 4.7: Control Implementation of Grid Side Converter with SMC approach [30]

4.8. Control Implementation using Integral Terminal Sliding mode control:

Now we shall discuss about ITSMC approach and its implementation in RSC and GSC converter. The basics has been discussed in chapter 3. Now we shall discuss it in detail by applying and manipulating system equations.

4.8.1. Rotor Side Converter topology for Integral Terminal Sliding mode control:

The sliding surfaces can be taken as:

$$s_{dr} = e_{dr} + \alpha_{dr} e_{Idr} \quad (94)$$

$$s_{qr} = e_{qr} + \alpha_{qr} e_{Iqr} \quad (95)$$

And the errors are taken as:

$$e_{dr}(t) = I_{dr} - I_{dr\_ref} \quad (96)$$

$$e_{qr}(t) = I_{qr} - I_{qr\_ref} \quad (97)$$

$$e_{Idqr} = \int_0^t \text{sign}(e_{dqr}(t))dt \quad (98)$$

Here α_{dr} and α_{qr} are positive constants chosen to guarantee the convergence of the steady-state d–q components errors to zero.

$$\dot{s}_{dr} = \dot{e}_{dr}(t) + \alpha_{dr}\dot{e}_{Idr}(t) \quad (99)$$

$$\dot{s}_{qr} = \dot{e}_{qr}(t) + \alpha_{qr}\dot{e}_{Iqr}(t) \quad (100)$$

Now putting the values of $\dot{I}_{dr}$ and $\dot{I}_{qr}$ in the equation (99) and (100):

$$\begin{bmatrix}\dot{s}_{dr}\\ \dot{s}_{qr}\end{bmatrix} = \frac{1}{\sigma L_r}\begin{bmatrix} -R_r I_{dr} + sw_s \sigma L_r I_{qr} - \frac{L_m}{L_s}\frac{d\lambda_s}{dt} \\ -R_r I_{qr} - sw_s \sigma L_r I_{dr} - \frac{L_m}{L_s} sw_s \lambda_s \end{bmatrix} + \begin{bmatrix}\alpha_{dr}\dot{e}_{Idr}(t)\\ \alpha_{qr}\dot{e}_{Iqr}(t)\end{bmatrix} + \begin{bmatrix}\dot{I}_{dr\_ref}(t)\\ \dot{I}_{qr\_ref}(t)\end{bmatrix} + \begin{bmatrix}\frac{1}{\sigma L_r} & 0\\ 0 & \frac{1}{\sigma L_r}\end{bmatrix}\begin{bmatrix}V_{dr}\\ V_{qr}\end{bmatrix} \quad (101)$$

Denoting $(-R_r I_{dr} + sw_s \sigma L_r I_{qr} - \frac{L_m}{L_s}\frac{d\lambda_s}{dt}) = F_{dr}$ and, $(-R_r I_{qr} - sw_s \sigma L_r I_{dr} - \frac{L_m}{L_s} sw_s \lambda_s) = F_{qr}$, we get:

$$\begin{bmatrix}\dot{s}_{dr}\\ \dot{s}_{qr}\end{bmatrix} = \begin{bmatrix} F_{dr} + \alpha_{dr}\dot{e}_{Idr}(t) + \dot{I}_{dr\_ref}(t) \\ F_{qr} + \alpha_{qr}\dot{e}_{Iqr}(t) + \dot{I}_{qr\_ref}(t) \end{bmatrix} + G_e \begin{bmatrix} V_{dr}\\ V_{qr}\end{bmatrix} \quad (102)$$

$$\begin{bmatrix} V_{dr}\\ V_{qr}\end{bmatrix} = -G_r{}^{-1} \begin{bmatrix} F_{dr} + \alpha_{dr}\dot{e}_{Idr}(t) + \dot{I}_{dr\_ref}(t) + U_{ndr} \\ F_{qr} + \alpha_{qr}\dot{e}_{Iqr}(t) + \dot{I}_{qr\_ref}(t) + U_{nqr} \end{bmatrix} \quad (103)$$

Where, U_{ndr} and U_{nqr} (Switching control law) can be given as:

$$\begin{bmatrix} U_{ndr}\\ U_{nqr}\end{bmatrix} = \begin{bmatrix} s_{dr} + K_{dr}\,\mathrm{sign}(s_{dr}) \\ s_{dr} + K_{qr}\,\mathrm{sign}(s_{qr}) \end{bmatrix} \quad (104)$$

And, the gain values should be taken as:

$$\begin{bmatrix} K_{dr}\\ K_{qr}\end{bmatrix} > \begin{bmatrix} \eta + \Delta F_{dr} \\ \eta + \Delta F_{dr} \end{bmatrix} + (1-\delta^{-1}) \begin{bmatrix} F_{dr} + \alpha_{dr}\dot{e}_{Idr}(t) + \dot{I}_{dr\_ref}(t) \\ F_{qr} + \alpha_{qr}\dot{e}_{Iqr}(t) + \dot{I}_{qr\_ref}(t) \end{bmatrix} \quad (105)$$

Where $|\Delta F_{dqr}| \leq \partial$, and $\delta^{-1} \leq G_r G_d{}^{-1} \leq \delta$ $(\delta > 1)$ are the uncertainty bounds.[39]

From [39], we can check the stability condition for the sign based ITSMC system. It satisfies the Lyapunov function $\dot{V}_{dqr} \leq -\eta\,|S_{dqr}|$. Since, $S_{dqe}(0) = 0$ and $\dot{V}_{dqr} \leq -\eta\,|S_{dqr}|$, system states are always remained on the terminal sliding surface $S_{dqe}(t) = 0$.

The integral terminal sliding variable S_{dqr} will then reach the sliding manifold $S = \dot{S} = 0$ in finite time. The gains K_{dqr} can be chosen to ensure the convergence of the sliding manifolds to zero in finite time [39], [54].

Remarks: The characteristics of the ITSMC can be explained as follows.

1) The finite convergence time can be chosen as follows:

$S_{dqe} = 0$; $T = |e_{Idqe}(0)| = |e_{dqe}(0)|/\alpha$.

2) In contrast to traditional TSMC, the singular problem does not happen on the control law.

2) Unlike normal TSMC, the singularity problem does not occur on the control law here.

3) Fast response can be achieved.

4) The gain K_{dqr} only depends on the limits of the feedforward signals and the uncertainty bound. Hence, it can be selected by some adaptation algorithm when upper bound of uncertainty is specified.

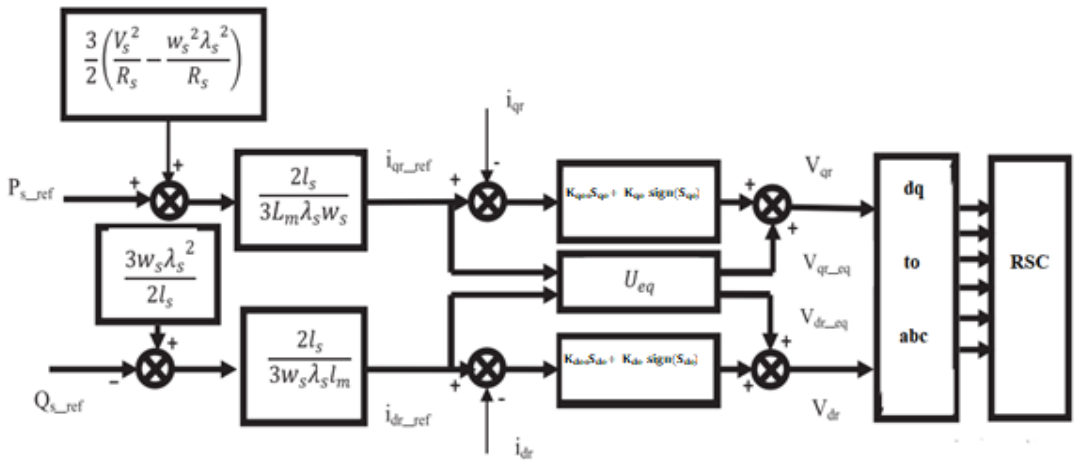

Figure 4.8: Control Implementation of Rotor Side Converter with ITSMC approach

4.8.2. Grid Side Converter topology for Integral Terminal Sliding mode control:

The main control objective of the GSC is to regulate the dc link of the DFIG. In addition, it may also help decrease the swings of the DFIG's total active and reactive power entering the grid. It is necessary to control the GSC so as to obtain constant dc voltage and enhance the DFIG performance. The voltage equations illustrating the behaviour of the GSC in the synchronously rotating frame (*d–q*) are given by (81) and (82).

The sliding Surfaces can be taken as:

$$s_{dg} = e_{dg} + \alpha_{dg} e_{Idg} \quad (106)$$

$$s_{qg} = e_{qg} + \alpha_{qg} e_{Iqg} \quad (107)$$

Where the errors are defined as:

$$e_{dg}(t) = I_{dg} - I_{dg\_ref} \quad (108)$$

$$e_{qg}(t) = I_{qg} - I_{qg\_ref} \quad (109)$$

$$e_{Idqg} = \int_0^t \text{sign}(e_{dqg}(t))dt \quad (110)$$

where α_{dg} and α_{qg} are positive constants chosen to guarantee the convergence of the steady-state *d–q* components errors to zero.

$$\dot{s}_{dg} = \dot{e}_{dg}(t) + \alpha_{dg}\dot{e}_{Idg}(t) \quad (111)$$

$$\dot{s}_{qg} = \dot{e}_{qg}(t) + \alpha_{qg}\dot{e}_{Iqg}(t) \quad (112)$$

$$\begin{bmatrix}\dot{s}_{dg}\\ \dot{s}_{qg}\end{bmatrix} = \frac{1}{L_f}\begin{bmatrix}V_{ds} - R_f I_{df} + w_s L_f I_{qf}\\ V_{qs} - R_f I_{qf} - w_s L_f I_{df}\end{bmatrix} + \begin{bmatrix}\alpha_{dg}\dot{e}_{Idg}(t)\\ \alpha_{qg}\dot{e}_{Iqg}(t)\end{bmatrix} + \begin{bmatrix}\dot{I}_{dg\_ref}(t)\\ \dot{I}_{qg\_ref}(t)\end{bmatrix} + \begin{bmatrix}\frac{1}{L_f} & 0\\ 0 & \frac{1}{L_f}\end{bmatrix}\begin{bmatrix}V_{df}\\ V_{qf}\end{bmatrix} \quad (113)$$

Denoting $V_{ds} - R_f I_{df} + w_s L_f I_{qf} = F_{dg}$ and $V_{qs} - R_f I_{qf} - w_s L_f I_{df} = F_{qg}$, we get:

$$\begin{bmatrix}\dot{s}_{dg}\\ \dot{s}_{qg}\end{bmatrix} = \begin{bmatrix}F_{dg} + \alpha_{dg}\dot{e}_{Idg}(t) + I_{df\_ref}(t)\\ F_{qg} + \alpha_{qg}\dot{e}_{Iqg}(t) + I_{qf\_ref}(t)\end{bmatrix} + G_g\begin{bmatrix}V_{df}\\ V_{qf}\end{bmatrix} \quad (114)$$

$$\text{Where, } G_g = \begin{bmatrix}\frac{1}{L_f} & 0\\ 0 & \frac{1}{L_f}\end{bmatrix}$$

$$\begin{bmatrix}V_{df}\\ V_{qf}\end{bmatrix} = -G_g^{-1}\begin{bmatrix}F_{dg} + \alpha_{dg}\dot{e}_{Idg}(t) + \dot{I}_{df\_ref}(t) + U_{ndg}\\ F_{qg} + \alpha_{qg}\dot{e}_{Iqg}(t) + \dot{I}_{qf\_ref}(t) + U_{nqg}\end{bmatrix} \quad (115)$$

Where, U_{ndg} and U_{nqg} (Switching control law) can be given as:

$$\begin{bmatrix}U_{ndg}\\ U_{nqg}\end{bmatrix} = \begin{bmatrix}s_{dg} + K_{dg}\,\text{sign}(s_{dg})\\ s_{dg} + K_{qg}\,\text{sign}(s_{qg})\end{bmatrix} \quad (116)$$

And the gain values can be taken as [22]:

$$\begin{bmatrix}K_{dg}\\ K_{qg}\end{bmatrix} > \begin{bmatrix}\eta + \Delta F_{dg}\\ \eta + \Delta F_{dg}\end{bmatrix} + (1-\delta^{-1})\begin{bmatrix}F_{dg} + \alpha_{dg}\dot{e}_{Idg}(t) + \dot{I}_{df\_ref}(t)\\ F_{qg} + \alpha_{qg}\dot{e}_{Iqg}(t) + \dot{I}_{qf\_ref}(t)\end{bmatrix} \quad (117)$$

Where $|\Delta F_{dqg}| \leq \partial$, and $\delta^{-1} \leq G_g G_d^{-1} \leq \delta$ $(\delta > 1)$ are the uncertainty bound.

From [39], we can check the stability condition for the sign based ITSMC system. It satisfies the Lyapunov function $\dot{V}_{dqg} \leq -\eta\,|S_{dqg}|$. Since, $S_{dqg}(0) = 0$ and $\dot{V}_{dqg} \leq -\eta\,|S_{dqg}|$, the system states are always remained on the terminal sliding surface $S_{dqe}(t) = 0$. [39], [54]

Remarks: The characteristics of the ITSMC can be explained as follows.

1) The finite convergence time can be chosen as follows:

$$S_{dqg} = 0;\ T = |e_{Idqg}(0)| = |e_{dqg}(0)|/\alpha.$$

2) In contrast to traditional TSMC, the singular problem does not happen on the control law.

3) Fast Convergence achieved.

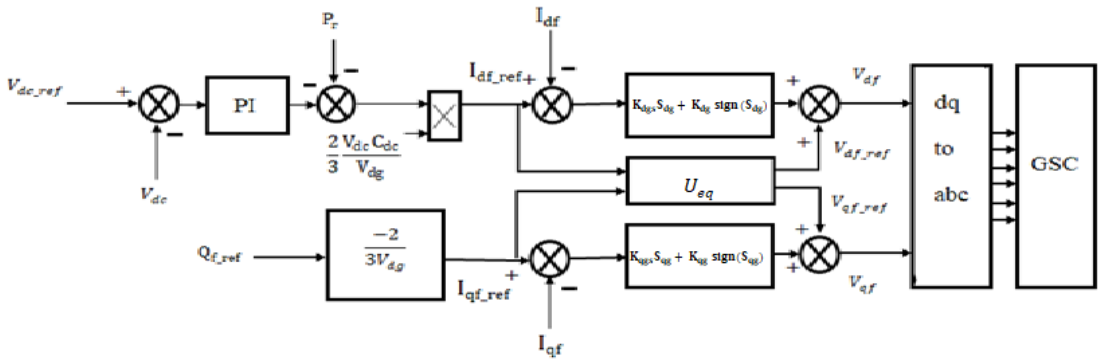

Figure 4.9: Control Implementation of Grid Side Converter with ITSMC approach

4.9. Chapter Summary:

In this chapter, we have discussed both DFIG and wind turbine mathematical model rigorously. The DFIG stator equations are expressed and analysed in synchronously rotating dq reference frame and furthermore, the equations are mathematically manipulated to design suitable SMC or ITSMC controllers. Similarly, DFIG grid filter model is also analysed in dq reference frame and mathematically manipulated for SMC and ITSMC controller. The objective of this is to generate reference voltage to control the RSC and GSC with suitable PWM technique.

Chapter 5

Simulation

5.1. Introduction:

In this chapter, we shall implement the simulations for a specified test condition on 3 different types of control schemes on DFIG based wind turbine namely conventional PI controller, sliding mode control and the proposed integral terminal sliding mode control in the MATLAB/SIMULINK software. Also, we shall check how the results alter with the incorporation of a crowbar. The results of different control schemes are compared and analysed in detail in this chapter.

5.2. Model Description of DFIG:

The test simulation is basically a part of microgrid, where the line voltage is 580 volts. From simscape library of MATLAB/SIMULINK, the block "Asynchronous machine in SI units" is used to model the Doubly fed induction generator for thesis. According to the block, the stator part can be connected direct to the grid and the rotor part is connected to the grid via back-to-back converters. There is a DC link capacitor in between the rotor and grid side converters. The switches for back-to-back converters are taken as IGBT/Diode switches. The grid side converter is connected to the grid with the help of a low pass RL filter. A crowbar is connected across rotor terminal so that high transient overcurrent during fault can bypass through it.

For control purpose of Rotor side and grid side converters, 2 separate subsystems are created where different control schemes are utilised as per the mathematical analysis done in previous chapters. These controllers generate gate pulse for the IGBT switches of the converters. Several measurement blocks are used in order to measure parameter values. The machine data (dq axis voltage, current and speed) are measured from the measurement port of the machine with the help of a bus selector. The machine torque is obtained from the aerodynamic torque generated from the wind turbine block.

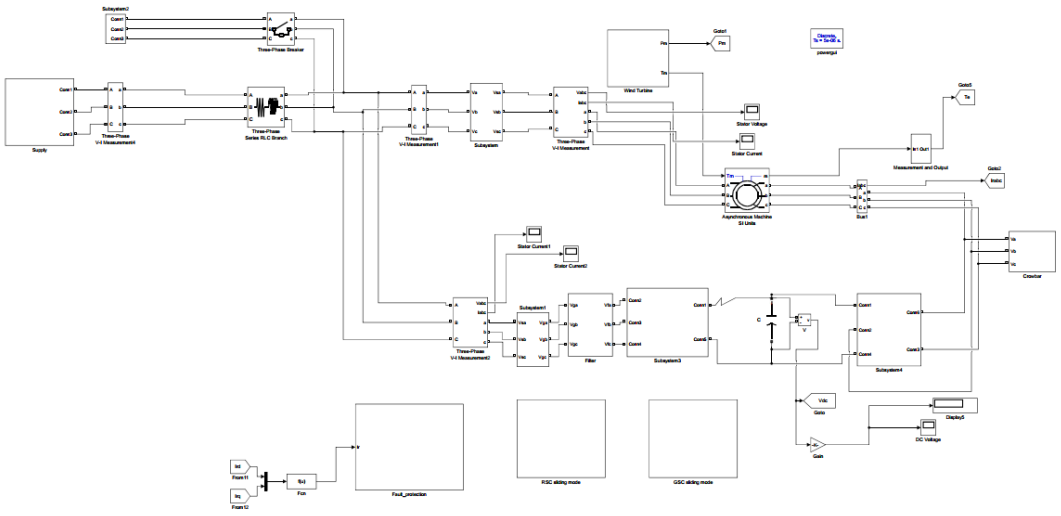

Figure 5.1. MATLAB/SIMULINK Block diagram for simulation of fault ride through with different controllers

The data for Doubly fed induction generator are listed in the following table:

Parameters	**Values**
Number of pole Pairs	2
Power Rating	0.96 MW
Stator Voltage	580 Volts
Rotor Voltage	580 Volts
Stator Resistance	0.0026 Ω
Stator Inductance	0.077 mH
Mutual Inductance	2.5 mH

Rotor Resistance	0.0029 Ω
Rotor Inductance	0.083 mH
Inertia	25 kg/m^2
Friction Factor	0.024
Filter Resistance	0.19864 mΩ
Filter Inductance	0.05261 mH
DC capacitor value	30000 μF
Crowbar Resistance	1 $\mu\Omega$

Table 5.1: Doubly Fed Induction generator and grid parameter values

5.3. Wind Turbine Aerodynamics Block:

The wind turbine block is made by utilising the equations of wind turbine as mentioned in chapter 4. The output of wind turbine is mechanical power and aerodynamic torque. The Torque is fed to the induction generator. The wind Turbine model uses wind speed, generator speed and the pitch angle as the input parameters. The radius of the blade, and the wind speed is used to derive the power coefficient Cp (λ, β). Then, the torque calculated. The figure below shows the block which performs the aerodynamic calculation of the turbine torque.

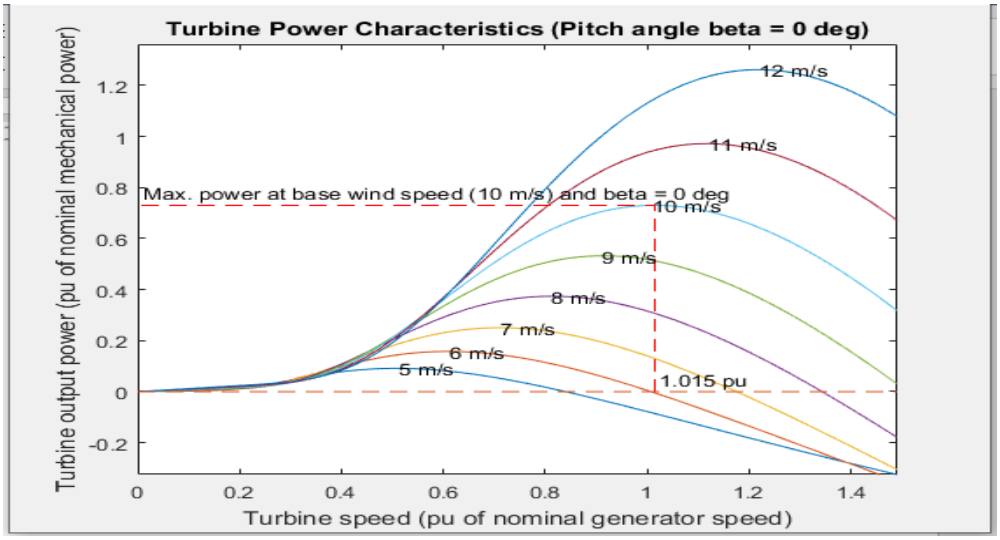

Figure 5.2. Wind Turbine Power characteristics

The optimum value of lambda is obtained from the Cp (λ, β) and tip to speed ratio curve. The optimum value of the power coefficient is the maximum value obtained from the curve and it is obtained to be 41% .

Parameters	Values
Wind Speed	10 m/s.
Power rating	0.96 MW
Radius	35 m
Pitch Angle	0°
Gear Ratio	80
Density of Wind	1.225 kg/m^3

Table 5.2: Wind Turbine parameter values

5.4. Simulation Test Scenario and Results:

Now we shall focus on our simulation work. To check the fault ride through capability with different types controllers, we have to introduce a fault in the grid side so that voltage dip occurs. Voltage dip is a sudden drop of the voltage at a point in the electrical system between 10% and 100% and lasts for some time. Three-phase symmetrical faults are most common and most dangerous type of voltage sags. In this work, we have introduced three phase symmetrical fault which results in a 100% dip of voltage in the DFIG grid side which implies that grid voltage becomes 0 that remains from 0.9 s to 1.1 s in the simulation runtime. A three-phase breaker is used purposefully to create the voltage dip on the aforementioned time interval.

The simulation runtime is 2 second. The following figures represents the voltage waveform for the time interval with fault condition, normal stator current waveform and normal rotor current waveform respectively.

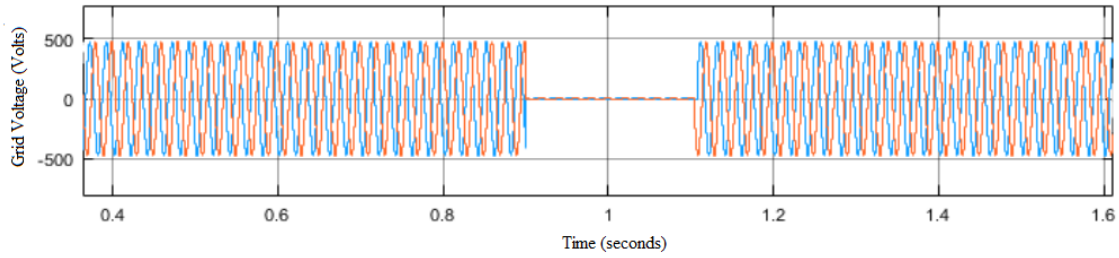

Figure 5.3: Grid voltage waveform with fault applied

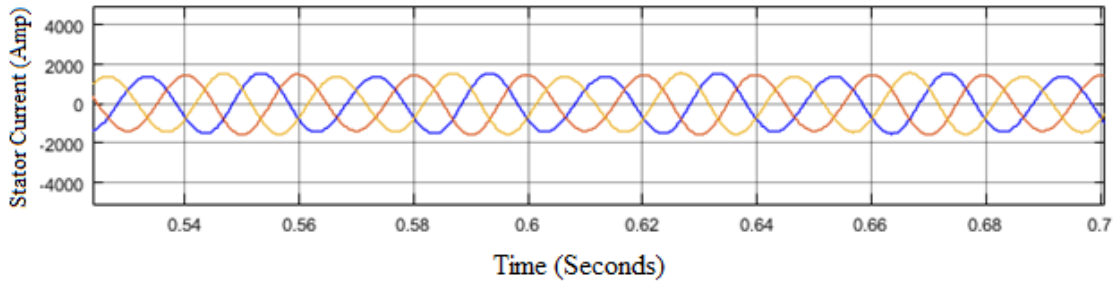

Figure 5.4. Normal value of stator current

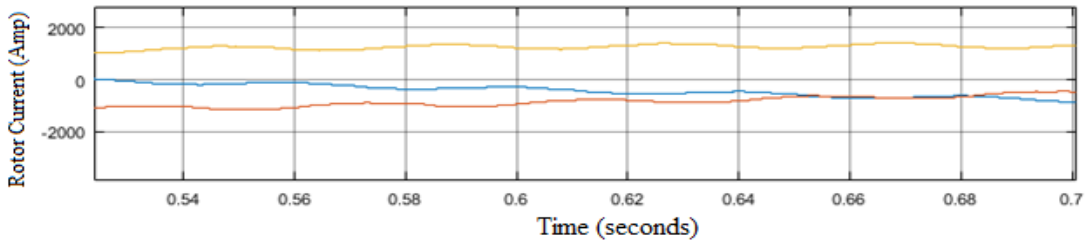

Figure 5.5. Normal value of Rotor current

5.4.1. Fault Ride Through Check Using Conventional PI controller:

Now we have to check the fault ride through capability using different controllers. First, we shall discuss about conventional PI control approach. This control approach implementation is done in Rotor Side converter and grid side converter control block in the system model in SIMULINK. The mathematical implementation of the control is done as per the control methodology discussed in the chapter 4. K_p and K_i values for the controllers are calculated as per the equations derived.

With this controller we have checked the response of Stator current, Rotor Current, Rotor Speed, Stator Active Power, Stator Reactive Power and Torque during the fault condition.

From the graphs it can be seen that as soon as 0.9 sec time reached, the three phase fault initiates, resulting in a spike in stator and rotor current, and a fluctuation in torque, that eventually stabilizes at zero. Active and Reactive Power becomes zero at fault time because the Voltage is 0. Again after 1.1 sec, a huge transient occurs in stator and rotor current, a fluctuation occurs in active, reactive power and torque. This method offers poor control in eliminating harmonics from the system and yield poor output, even in steady state.

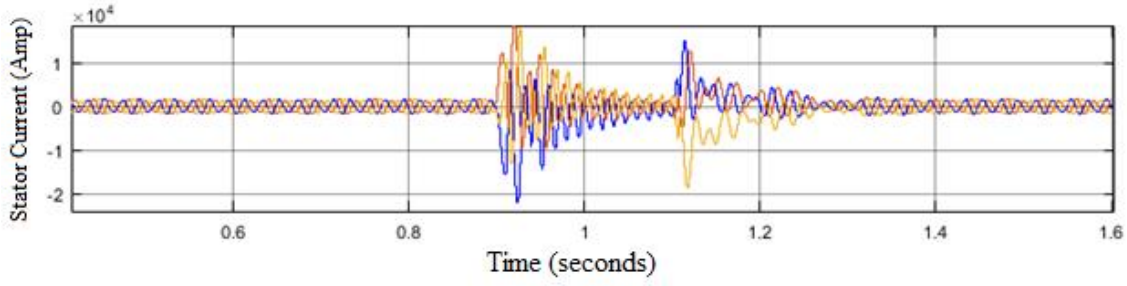

Figure 5.6.1: Stator Current Variation in Conventional PI Controller

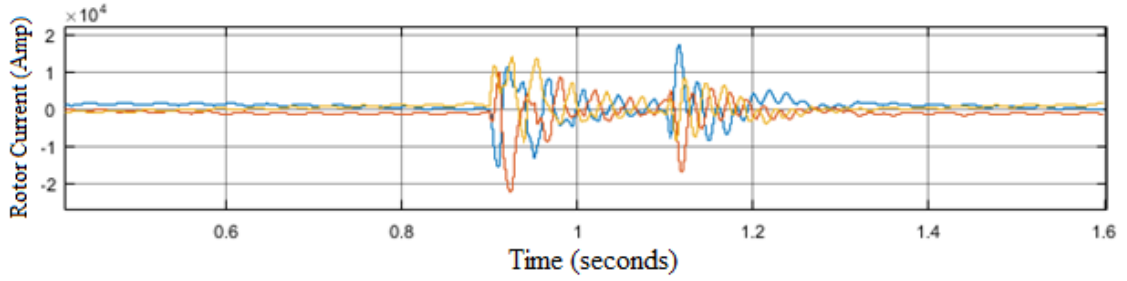

Figure 5.6.2: Rotor Current Variation in Conventional PI Controller

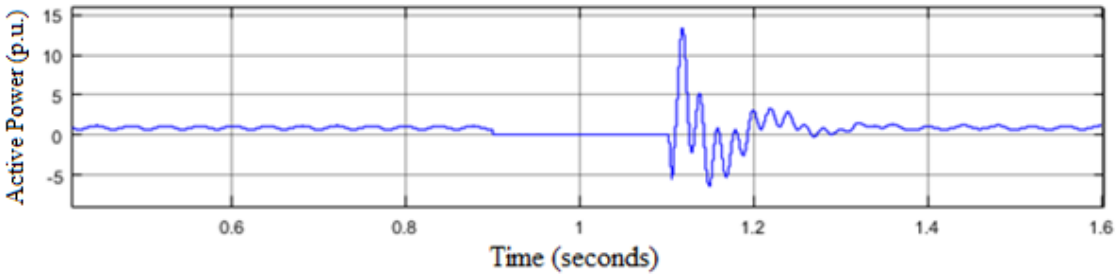

Figure 5.6.3: Stator Active Power Variation in Conventional PI Controller

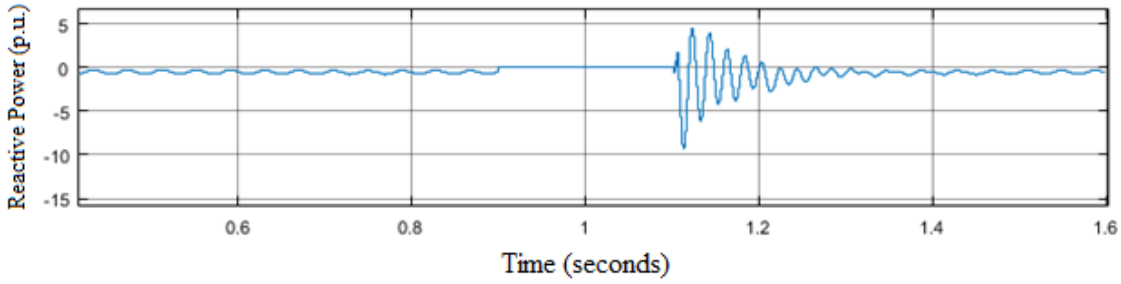

Figure 5.6.4: Stator Reactive Power Variation in Conventional PI Controller

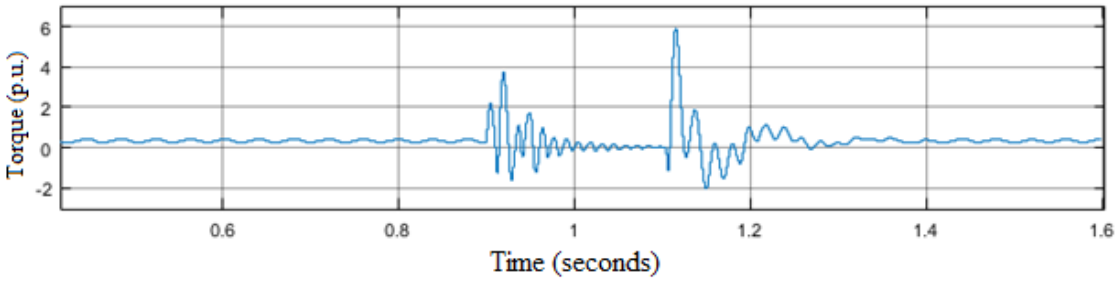

Figure 5.6.5: Torque Variation in Conventional PI Controller

5.4.2. Fault Ride Through Check Using Sliding Mode Control:

Now we have to check the fault ride through capability using 1st order sliding mode control. This control approach implementation is done in Rotor Side converter and grid side converter control block in the system model in SIMULINK. The detailed mathematical expressions of 1st order sliding mode control scheme are presented in chapter 3 and 4.

Similar to PI controller, now we have to check the response of Stator current, Rotor Current, Rotor Speed, Stator Active Power, Stator Reactive Power and Torque during the fault condition.

From the graphs it can be seen that as soon as 0.9 sec time reached, the three phase fault initiates, resulting in a spike in stator and rotor current, and a fluctuation in torque, that eventually stabilizes at zero. Active and Reactive Power becomes zero at fault time because

the Voltage is 0. Again after 1.1 sec, a huge transient occurs in stator and rotor current, a fluctuation occurs in active, reactive power and torque. From the waveforms it can be concluded that the response is better than PI controller in terms of lesser harmonics in steady state. But the high frequency chattering is present in the outputs. The outputs are shown below:

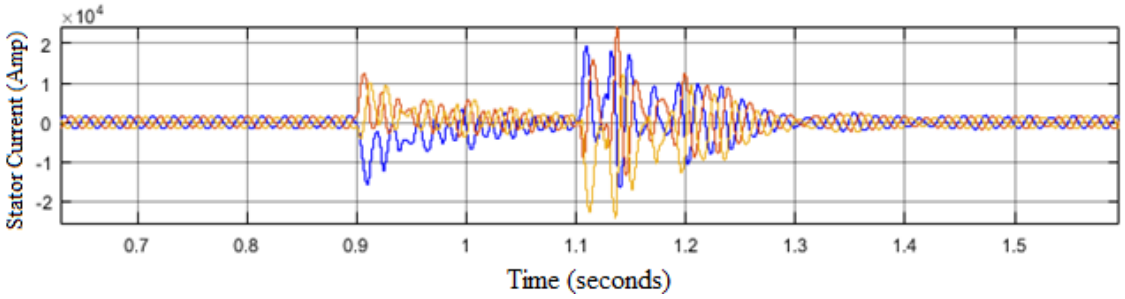

Figure 5.7.1: Stator Current Variation in Sliding Mode Controller

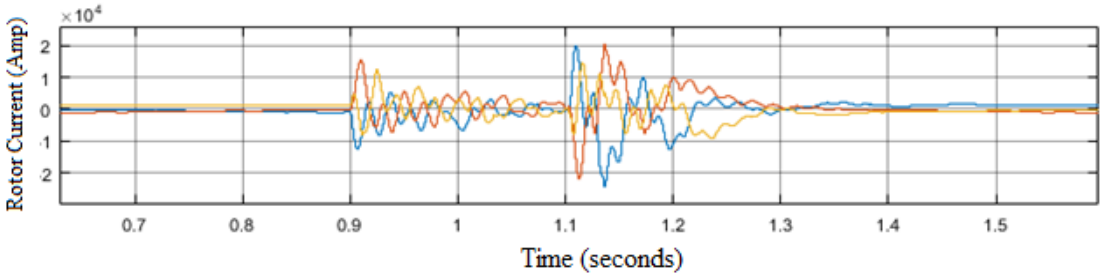

Figure 5.7.2: Rotor Current Variation in Sliding Mode Controller

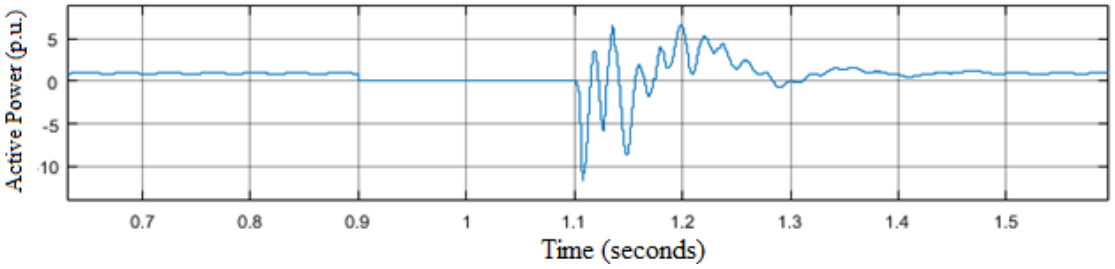

Figure 5.7.3: Active Power Variation in Sliding mode Controller

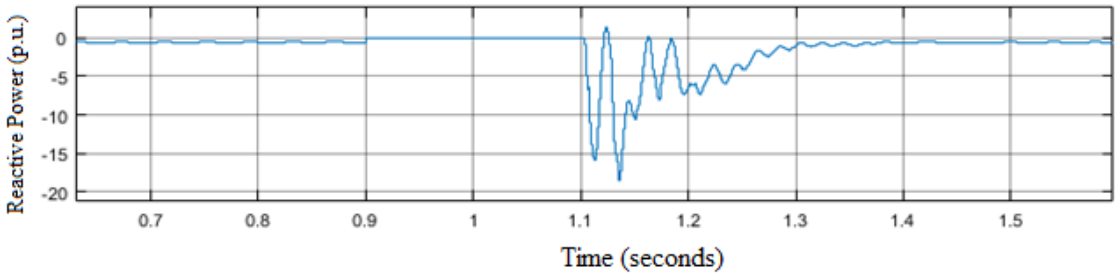

Figure 5.7.4. Reactive Power Variation in Sliding mode Controller

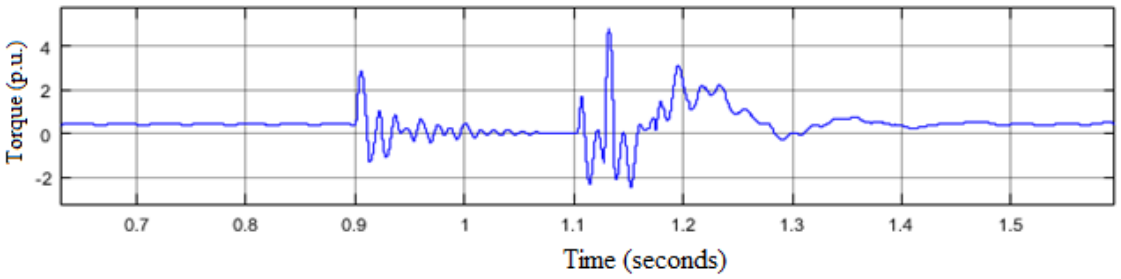

Figure 5.7.5: Torque Variation in Sliding mode Controller

5.4.3. Fault Ride Through Check Using Integral Terminal Sliding Mode Control:

Now we have to check the fault ride through capability using the proposed Integral Terminal sliding mode control. This control approach implementation is done in Rotor Side converter and grid side converter control block in the system model in SIMULINK. The detailed mathematical expressions of Integral Terminal sliding mode control. scheme is presented in chapter 3 and 4.

Similar to other two controllers, now we have to check the response of Stator current, Rotor Current, Rotor Speed, Stator Active Power, Stator Reactive Power and Torque during the fault condition using integral terminal sliding mode control.

From the graphs it can be seen that as soon as 0.9 sec time reached, the three phase fault initiates, resulting in a spike in stator and rotor current, and a fluctuation in torque, that eventually stabilizes at zero. Active and Reactive Power becomes zero at fault time because the Voltage is 0. Again after 1.1 sec, a transient occurs in stator and rotor current, a fluctuation occurs in active, reactive power and torque. The nature of the graphs are shown below:

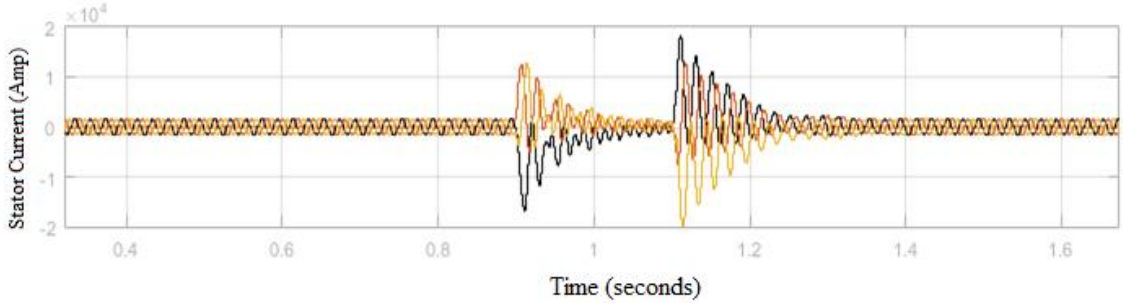

Figure 5.8.1: Stator Current Variation in Integral Terminal Sliding Mode Controller

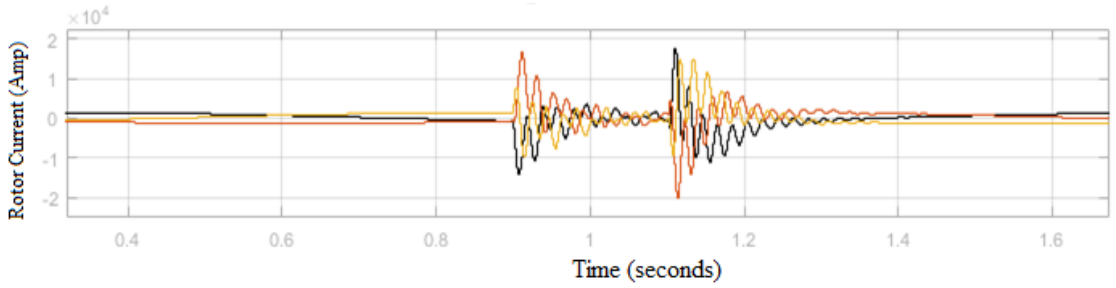

Figure 5.8.2: Rotor Current Variation in Integral Terminal Sliding Mode Controller

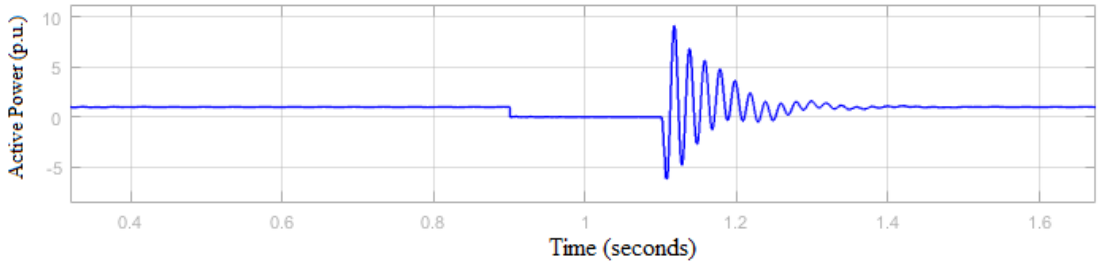

Figure 5.8.3: Active Power Variation in Integral Terminal Sliding Mode Controller

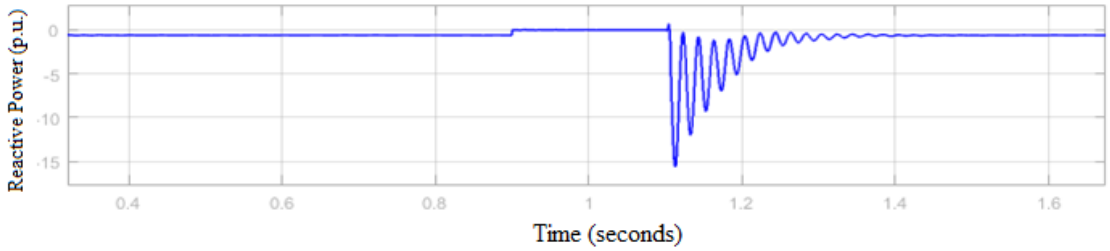

Figure 5.8.4: Reactive Power Variation in Integral Terminal Sliding Mode Controller

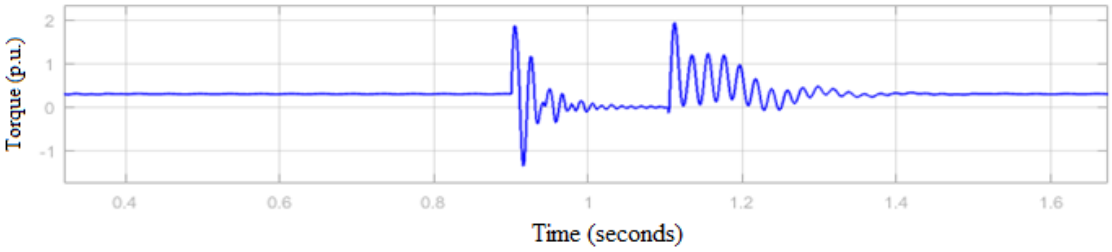

Figure 5.8.5: Torque Variation in Integral Terminal Sliding Mode Controller

5.5. Result Summary:

From the obtained results, PI controllers are yielding poor performance in steady state. We can see that the proposed integral terminal sliding mode control is much better in terms of eliminating the high frequency chattering effect that is exhibited by sliding mode control, and it is also capable of ensuring finite time convergence as compared to conventional sliding mode control, where we can see there is a tendency of yielding asymptotic stability. It is useful enough for the system to abide by the grid codes. However, there is a disadvantage in ITSMC that it cannot eliminate overshoot in transient period much.

5.5.1. Data Comparison Table:

Different Controllers	Maximum Overshoot of Stator current in transient period (pu)	Maximum Overshoot of Stator current in transient clearing period (pu)	Settling Time (Seconds)	Chattering
PI	12	10.85	0.25 sec	--
1st Order SMC	8.57	13.14	0.3 sec	Significant
ITSMC	9.14	11.42	0.15 sec	Almost none

Table 5.3: Comparison of Stator current transient characteristics in 3 different controllers

Different Controllers	Maximum Overshoot of Rotor current in transient period (pu)	Maximum Overshoot of Rotor current in transient clearing period (pu)	Settling Time (Seconds)	Chattering
PI	18.66	16	0.2 sec	--
1st Order SMC	14	19.6	0.18 sec	Significant
ITSMC	14	17.7	0.16 sec	Almost none

Table 5.4: Comparison of Rotor current transient characteristics in 3 different Controllers

Different Controllers	Maximum Overshoot in Stator Active Power in transient period (pu)	Maximum Overshoot in Stator Active Power in transient clearing period (pu)	Settling Time (Seconds)	Chattering
PI	0	13	>0.5 sec	--
1st Order SMC	0	11.5	>0.5 sec	Significant
ITSMC	0	9	0.22 sec	Almost none

Table 5.5: Comparison of Active Power transient characteristics in 3 different controllers

Different Controllers	Maximum Overshoot in Stator reactive power in transient period(pu)	Maximum Overshoot in Stator reactive power in transient clearing period (pu)	Settling Time (Seconds)	Chattering
PI	0	10	>0.5 sec	--
1st Order SMC	0	18	>0.5 sec	Significant
ITSMC	0	15.5	0.25 sec	Almost none

Table 5.6: Comparison of Reactive Power transient characteristics in 3 different controllers

Different Controllers	Maximum Overshoot of Torque in transient period(pu)	Maximum Overshoot of Torque in transient clearing period (pu)	Settling Time (Seconds)	Chattering
PI	3.9	6	>0.5 sec	--
1st Order SMC	2.9	4.6	>0.5 sec	Significant
ITSMC	1.92	2	0.25 sec	Almost none

Table 5.7: Comparison of Torque transient characteristics in 3 different controllers

5.6. Insertion of Crowbar:

Now our Task is to insert a crowbar in the system. The crowbar is a simple diode bridge that connects a resistor in its output. The purpose of crowbar is to bypass the excessive rotor current during fault period and to protect rotor windings to some extent.

For implementation of crowbar, the measured value of rotor current is compared with the reference values of rotor current. If the measured value exceeds two times the reference current, the crowbar IGBT switch activates and the crowbar starts to conduct.

Since we achieved poor control using PI based control, so from now, the comparison of SMC and ITSMC are presented only.

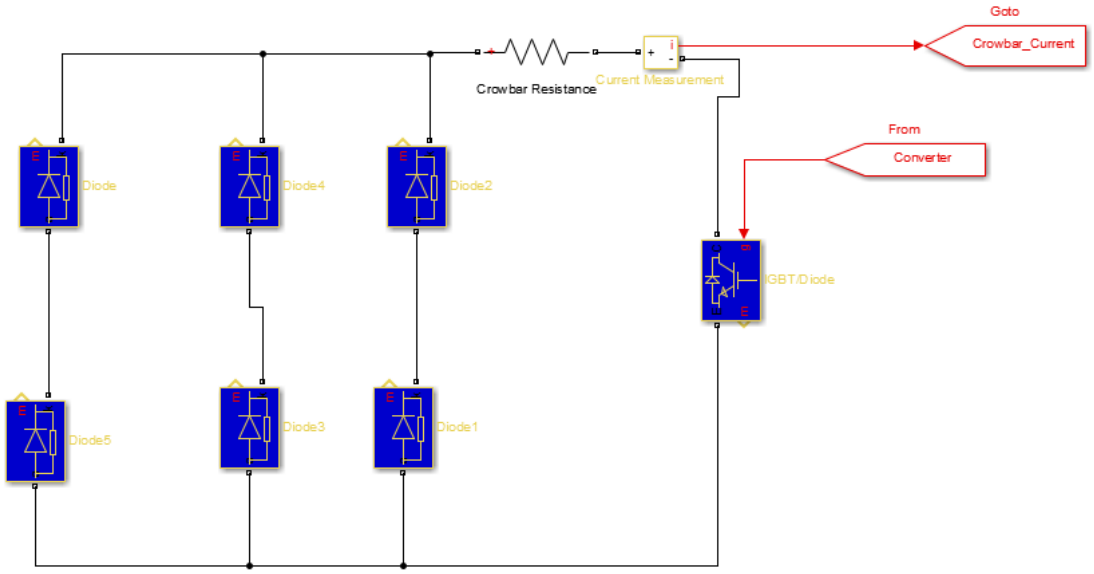

Figure 5.9: Crowbar circuit

5.6.1. 1st Order Sliding mode Control with crowbar:

Now, with the inclusion of crowbar circuit, Simulations with the help of Sliding Mode Controllers are shown here. The graphs for stator and rotor current, Active and Reactive Power and Torque are shown here.

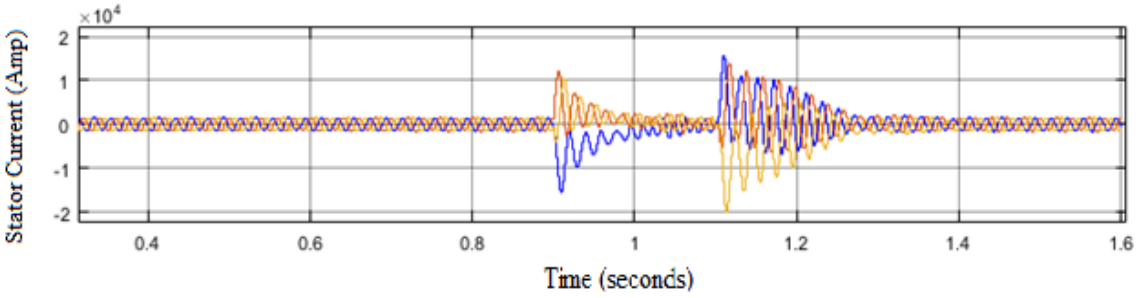

Figure 5.10.1: Stator Current variation in Sliding mode controller with Crowbar

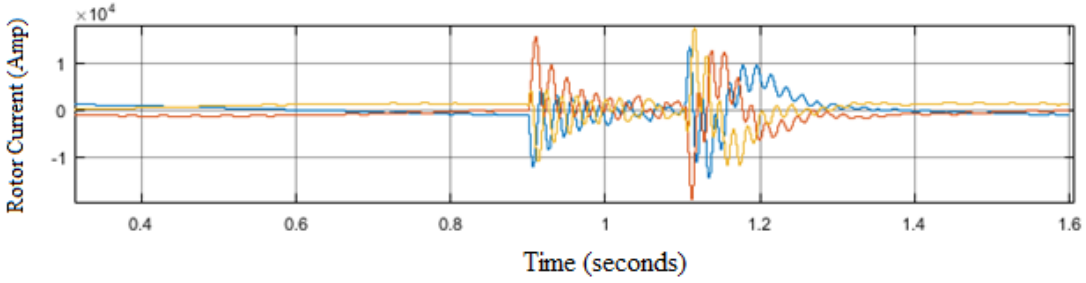

Figure 5.10.2: Rotor Current variation in Sliding mode controller with Crowbar

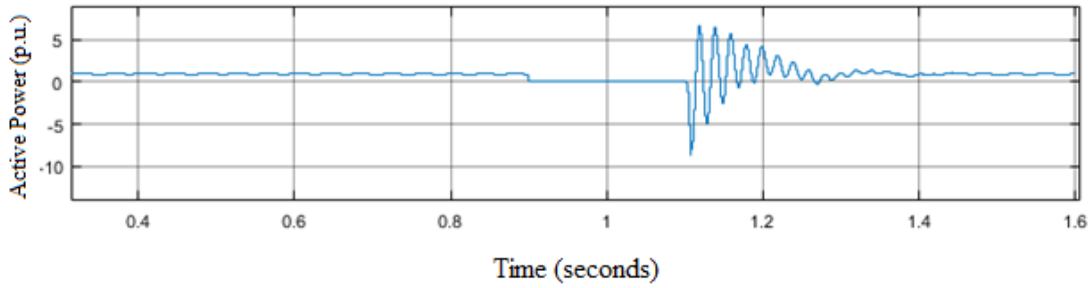

Figure 5.10.3: Active Power variation in Sliding mode controller with Crowbar

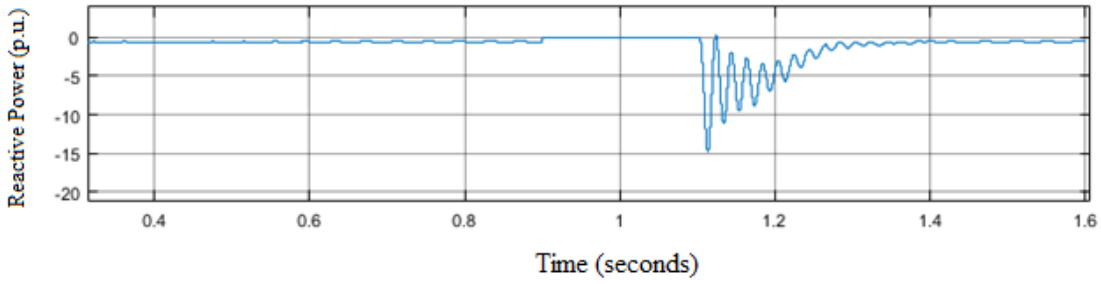

Figure 5.10.4: Reactive Power variation in Sliding mode controller with Crowbar

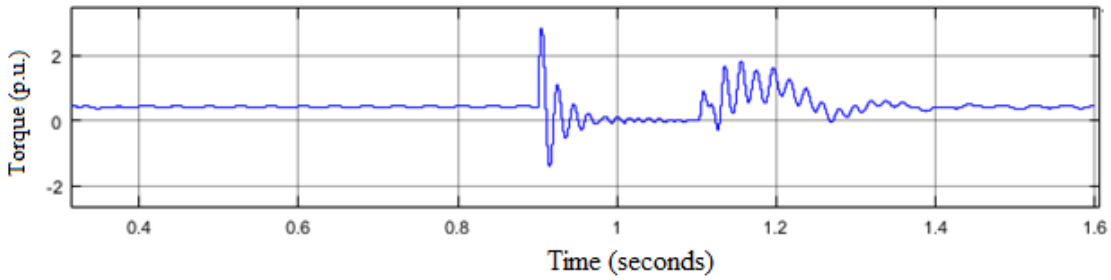

Figure 5.10.5: Torque variation in Sliding mode controller with Crowbar

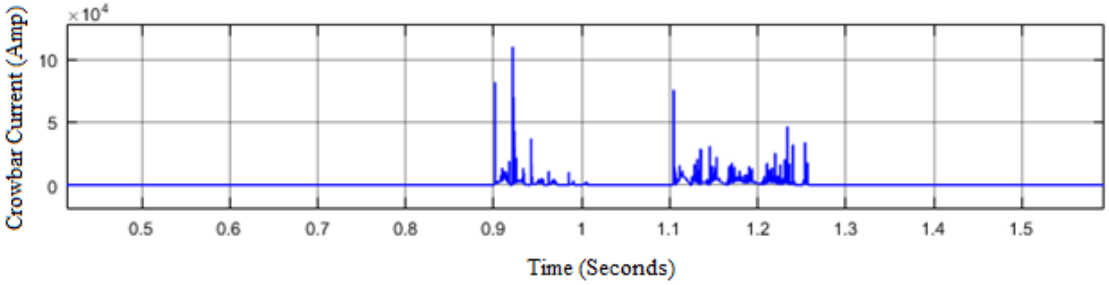

Figure 5.10.6: Crowbar Current in SMC approach

5.6.2. Integral Terminal Sliding Mode Control with crowbar:

Now we shall check the results of ITSMC controllers with crowbar. The results are listed below:

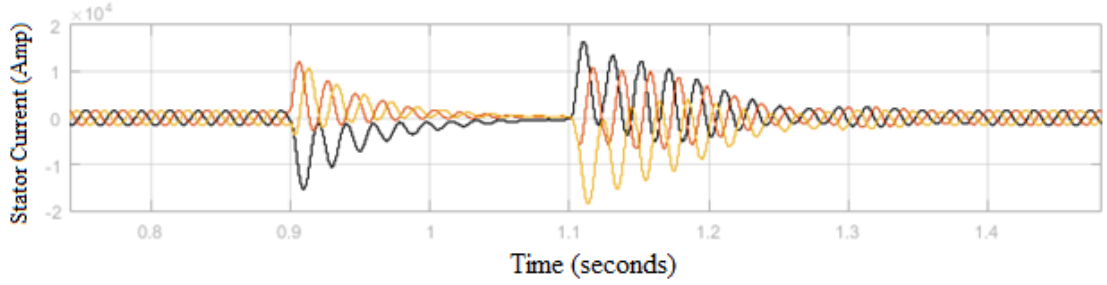

Figure 5.11.1: Stator Current variation in ITSMC controller with crowbar

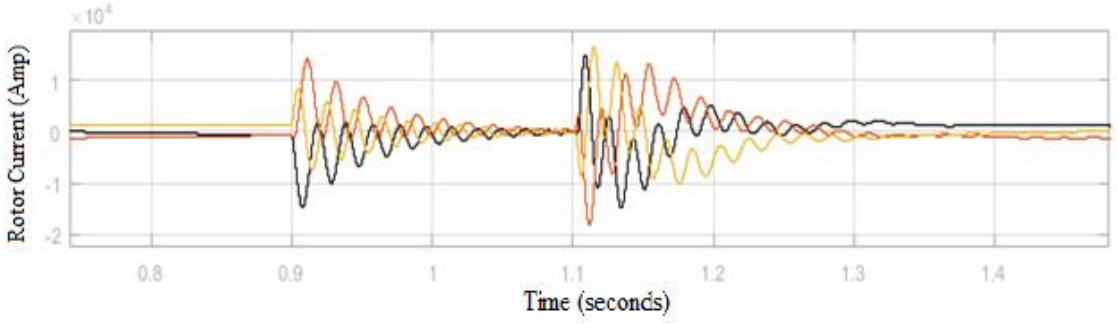

Figure 5.11.2: Rotor Current variation in ITSMC controller with crowbar

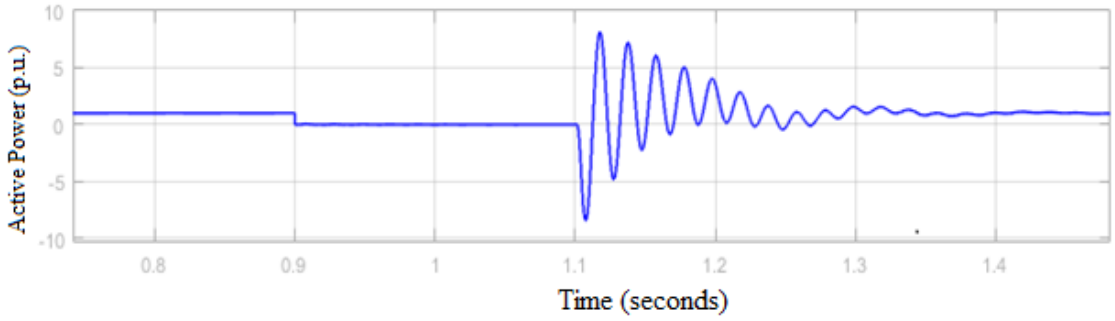

Figure 5.11.3: Active Power variation in ITSMC controller with crowbar

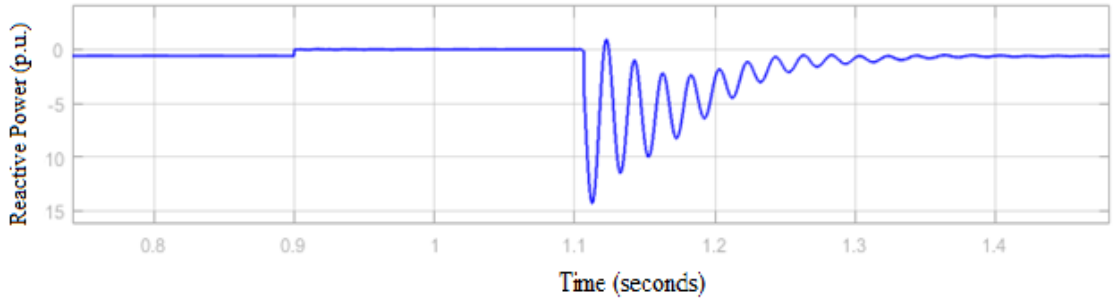

Figure 5.11.4: Reactive Power variation in ITSMC controller with crowbar

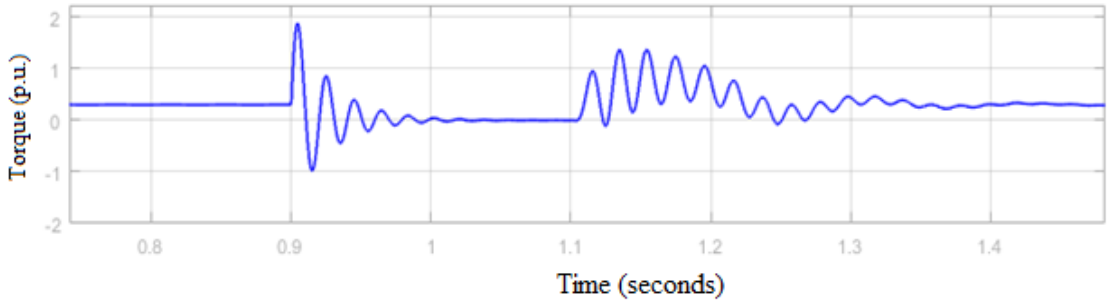

Figure 5.11.5: Torque variation in ITSMC controller with crowbar

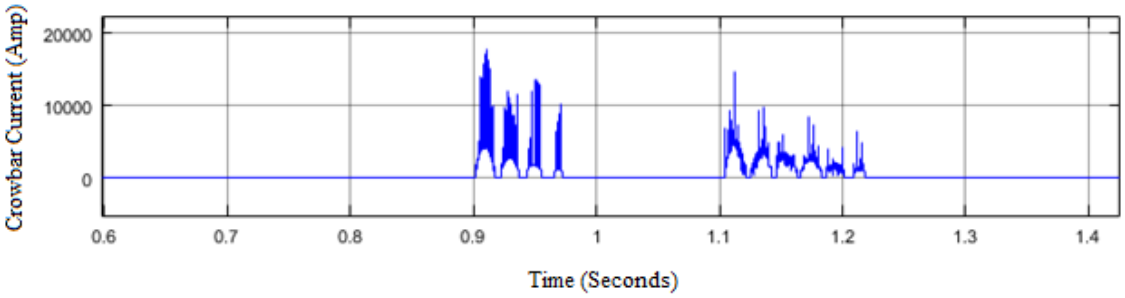

Figure 5.11.6: Crowbar Current in ITSMC approach

5.7. Result Summary:

From the obtained results, we can conclude that the inclusion of crowbar limits the high currents to certain extent. That improves the transient characteristics of the stator and rotor current. Also, this contributes in yielding better transient characteristics in torque, active and reactive power.

5.7.1. Data Table:

Different Controllers	Maximum overshoot of Stator current in transient period (pu)	Maximum overshoot of Stator current in transient clearing period (pu)	Settling Time (Seconds)	Chattering
1st Order SMC	8	11.43	0.2 sec	Present
ITSMC	8	10.28	0.15 sec	None

Table 5.8: Comparison of Stator current transient characteristics in 2 different controllers with crowbar

Different Controllers	Maximum overshoot of Rotor current in transient period (pu)	Maximum overshoot of Rotor current in transient clearing period (pu)	Settling Time (Seconds)	Chattering
1st Order SMC	12.44	16	0.2 sec	Present
ITSMC	12	15.11	0.17 sec	None

Table 5.9: Comparison of Rotor current transient characteristics in 2 different controllers with crowbar

Different Controllers	Maximum overshoot of Stator Active Power in transient period (pu)	Maximum overshoot of Stator Active Power in transient clearing period (pu)	Settling Time (Seconds)	Chattering
1st Order SMC	0	8.5	0.3 sec	Present
ITSMC	0	8	0.22 sec	None

Table 5.10: Comparison of Stator Active Power transient characteristics in 2 different controllers with crowbar

Different Controllers	Maximum overshoot of Stator Reactive Power in transient period (pu)	Maximum overshoot of Stator Reactive Power in transient clearing period (pu)	Settling Time (Seconds)	Chattering
1st Order SMC	0	15	0.32 sec	Present
ITSMC	0	14	0.25 sec	None

Table 5.11: Comparison of Stator Reactive Power transient characteristics in 2 different controllers with crowbar

Different Controllers	Maximum overshoot of Torque in transient period (pu)	Maximum overshoot of Torque in transient clearing period (pu)	Settling Time (Seconds)	Chattering
1st Order SMC	2.5	1.9	>0.5 sec	Present
ITSMC	1.9	1.3	0.25 sec	None

Table 5.12: Comparison of Torque transient characteristics in 2 different controllers with crowbar

5.8. Chapter Summary:

In this chapter, we have performed the simulation work. The results of conventional PI controller, SMC and ITSMC are analysed. Furthermore, we include a crowbar to the rotor terminals and run the simulation. It is seen that the results have been improved from PI to ITSMC, especially when steady state fluctuation is concerned. However, the chattering effect is seen on SMC based control but there is a significant reduction of chattering in ITSMC controller. Overshoots in Active power reactive power are also improved in ITSMC approach. The problem of high overshoot of currents in fault period is reduced to some extent when we apply crowbar in the circuit.

Chapter 6

Conclusion and Future Work

6.1. Conclusion:

In this thesis, a novel integral terminal sliding mode control approach is undertaken in order to enhance the fault ride through performance of DFIG based wind turbine. The objective of this thesis work is to meet the grid codes, improving the transient performance of the system and to ensure the finite time convergence of the system. 3 phase symmetrical fault with 100% voltage sag is used in order to check the fault ride through using the proposed controller. The obtained results ensure the terminal attractor property of integral terminal sliding mode control that alleviates the chattering phenomenon in 1^{st} order sliding mode control. Also, the due to the inherent property of the ITSMC controller, it yields better results than SMC and PI type controller in achieving a lesser settling time. Further, to reduce the current overshoot to some extent, we use a crowbar at rotor terminal and compare the compared result ensures the superiority of Integral terminal sliding mode control. However, Integral Terminal sliding mode control has the limitation that it cannot alleviate overshoot in a good amount. In fact, any software-based approach has this kind of limitations. For that, they should always be accompanied with some auxiliary hardware devices. However, properly tuning the gain values in respective control, certain amount of better result can be obtained.

6.2. Future Works:

Doubly Fed Induction Generator has a wide application in Wind energy conversion system. Being an emerging source of renewable energy, the application of wind energy is increasing day by day to replace the use of conventional energy sources. In microgrid applications, wind turbines are a main component, so does DFIG.

Grid connected Wind turbines are very prone to experience grid faults, be it symmetrical or asymmetrical. So, Fault analysis is very important to maintain grid codes and to protect DFIG power converters from high rotor current. Several works were presented in order to address grid fault in DFIG connected wind turbine. In this work our contribution is to present a novel ITSMC approach along with crowbar to limit the transients and ensure fast convergence. However, pure tuning of gain values of ITSMC can affect the output significantly. Fuzzy logic controller can be used for tuning the gains more appropriately. Also, This work further can be progressed by

applying more robust control methodologies like H-infinity control, Backstepping control or some observer design based method, like Sliding mode observer or Kalman Filter observer to estimate the error by mathematical derivation. Also some advanced hardware approaches that is of comparatively low cost but more efficient can be employed to limit the transients. Furthermore, for application in smart grid-based system, some AI methods also can be used which are proved to be more robust and reliable nowadays and are being applied in many applications.

References

[1] Z. Salameh, “Wind Energy Conversion Systems,” in *Renewable Energy System Design*, Elsevier, 2014, pp. 115–199.

[2] M. B. C. Salles, J. R. Cardoso, A. P. Grilo, C. Rahmann and K. Hameyer, "Control strategies of doubly fed induction generators to support grid voltage," 2009 IEEE International Electric Machines and Drives Conference, 2009, pp. 1551-1556, doi: 10.1109/IEMDC.2009.5075410.

[3] C. Wessels, F. Gebhardt, and F. W. Fuchs, “Fault ride-through of a DFIG wind turbine using a dynamic voltage restorer during symmetrical and asymmetrical grid faults,” *IEEE Trans. Power Electron.*, vol. 26, no. 3, pp. 807–815, 2011.

[4] Z. Du and W. Gu, “Aerodynamics analysis of wind power,” *WNWEC 2009 - 2009 World Non-Grid-Connected Wind Power Energy Conf.*, no. 1, pp. 235–237, 2009

[5] O. Noureldeen and I. Hamdan, “A novel controllable crowbar based on fault type protection technique for DFIG wind energy conversion system using adaptive neuro-fuzzy inference system,” *Prot. control mod. power syst.*, vol. 3, no. 1, 2018.

[6] C. Hamon, “Doubly-fed induction generator modeling and control in DigSilent power factory,” *Diva-portal.org*. [Online]. Available: https://www.diva-portal.org/smash/get/diva2:611644/FULLTEXT01.pdf. [Accessed: 20-Jun-2022].

[7] A. D. Bebars, A. A. Eladl, G. M. Abdulsalam, and E. A. Badran, “Internal electrical fault detection techniques in DFIG-based wind turbines: a review,” *Prot. control mod. power syst.*, vol. 7, no. 1, pp. 1–22, 2022.

[8] N. Espinoza and O. Carlson, “Field-test of wind turbine by voltage source converter,” *Wind Energy Sci.*, vol. 4, no. 3, pp. 465–477, 2019.

[9] D. Zhu, X. Zou, S. Zhou, W. Dong, Y. Kang, and J. Hu, “Feedforward current references control for DFIG-based wind turbine to improve transient control performance during grid faults,” *IEEE trans. energy convers.*, vol. 33, no. 2, pp. 670–681, 2018

[10] A. O. Ibrahim, N. Thanh-Hai, L. Dong-Choon, and K. Su-Chang, “A fault ride-through technique of DFIG wind turbine systems using dynamic voltage restorers,” *IEEE Trans. Energy Convers.*, vol. 26, no. 3, pp. 871-882, Sep. 2011.

[11] G. Wen, Y. Chen, Z. Zhong, and Y. Kang, “Dynamic voltage and current assignment strategies of nine-switch-converter-based DFIG wind power system for low-voltage ride-through (LVRT) under symmetrical grid

voltage dip," *IEEE Trans. Ind. Appl.*, vol. 52, no. 4, pp. 3422-3434, Jul./Aug. 2016

[12] W. Qiao, G. K. Venayagamoorthy, and R. G. Harley, "Real-Time implementation of a STATCOM on a wind farm equipped with doubly fed induction generators," *IEEE Trans. Ind. Appl.*, vol. 45, no. 1, pp. 98-107, Jan. 2009.

[13] P. S. Flannery, and G. Venkataramanan, "Unbalanced voltage sag ride-through of a doubly fed induction generator wind turbine with series grid-side converter," *IEEE Trans. Ind. Appl.*, vol. 45, no. 5, pp. 1879-1887, Sep./Oct. 2009.

[14] C. Wessels, F. Gebhardt, and F. W. Fuchs, "Fault ride-through of a DFIG wind turbine using a dynamic voltage restorer during symmetrical and asymmetrical grid gaults," *IEEE Trans., Power Electron.*, vol. 26, pp. 807-815, 2011.

[15] A. O. Ibrahim, T. H. Nguyen, D.-C. Lee, and S.-C. Kim, "A fault ride-through technique of DFIG wind turbine systems using dynamic voltage restorers," *IEEE trans. energy convers.*, vol. 26, no. 3, pp. 871–882, 2011.

[16] D. Ramirez, S. Martinez, C. A. Platero, F. Blazquez, and R. M. de Castro, "Low-voltage ride-through capability for wind generators based ondynamic voltage restorers," *IEEE Trans., Energy Convers.*, vol. 26, pp. 195-203, 2011

[18] M. Fazli, A. R. Shafighi, A. Fazli and H. A. Shayanfar, "Effects of STATCOM on wind turbines equipped with DFIGs during grid faults," 2010 World Non-Grid-Connected Wind Power and Energy Conference, 2010, pp. 1-4, doi: 10.1109/WNWEC.2010.5673205.

[19] G. Wen, Y. Chen, P. Zhang, and Y. Kang, "Nine-Switch-Converter-based DFIG Wind Power System and its dynamic port-current assigned approach for Low Voltage Riding Through (LVRT)," in *2015 IEEE Applied Power Electronics Conference and Exposition (APEC)*, 2015.

[20] G. Pannell, D. J. Atkinson, and B. Zahawi, "Minimum-threshold crowbar for a fault-ride-through grid-code-compliant DFIG wind turbine," *IEEE Trans. Energy Convers.*, vol. 25, no. 3, pp. 750-759, Sep. 2010.

[21] J. Morren, and S. W. H. de Haan, "Ridethrough of wind turbines with doubly-Fed induction generator during a voltage dip," *IEEE Trans. Energy Convers.*, vol. 20, no. 2, pp. 435-441, Jun. 2005.

[22] M. J. Morshed and A. Fekih, "A Fault-Tolerant Control Paradigm for Microgrid-Connected Wind Energy Systems," in *IEEE Systems Journal*, vol. 12, no. 1, pp. 360-372, March 2018, doi: 10.1109/JSYST.2016.2531718.

[23] R. Asghar, F. Rehman, Z. Ullah, A. Aman, K. Iqbal, and A. Ali Nawaz, "Modified switch type fault current limiter for low-voltage ride-through enhancement and reactive

power support of DFIG-WT under grid faults," *IET Renew. Power Gener.*, vol. 14, no. 9, pp. 1481–1490, 2020.

[24] S. Sahoo, A. Mishra, K. Chatterjee and C. K. Sharma, "Enhanced fault ride — Through ability of DFIG-based wind energy system using superconducting fault current limiter," 2017 4th International Conference on Power, Control & Embedded Systems (ICPCES), 2017, pp. 1-5, doi: 10.1109/ICPCES.2017.8117627.

[25] Zhang, X.-G & Xu, D.-G. (2009). Research on control of DFIG with active crowbar under symmetry voltage fault condition. 13. 99-103.

[26] R. Zhu, Z. Chen, X. Wu and F. Deng, "Virtual Damping Flux-Based LVRT Control for DFIG-Based Wind Turbine," in IEEE Transactions on Energy Conversion, vol. 30, no. 2, pp. 714-725, June 2015, doi: 10.1109/TEC.2014.2385966.

[27] R. Zhu, F. Deng, C. Zhe and M. Liserre, "Enhanced Control of DFIG Wind Turbine Based on Stator Flux Decay Compensation," 2018 IEEE Power & Energy Society General Meeting (PESGM), 2018, pp. 1-1, doi: 10.1109/PESGM.2018.8585761.

[28] D. Zhu, X. Zou, S. Zhou, W. Dong, Y. Kang and J. Hu, "Feedforward Current References Control for DFIG-Based Wind Turbine to Improve Transient Control Performance During Grid Faults," in IEEE Transactions on Energy Conversion, vol. 33, no. 2, pp. 670-681, June 2018, doi: 10.1109/TEC.2017.2779864.

[29] D. Zhu, X. Zou, L. Deng, Q. Huang, S. Zhou, and Y. Kang, "Inductance-emulating control for DFIG-based wind turbine to ride-through grid faults," *IEEE Trans. Power Electron.*, vol. 32, no. 11, pp. 8514–8525, 2017.

[30] N. H. Saad, A. A. Sattar, and A. E.-A. M. Mansour, "Low voltage ride through of doubly-fed induction generator connected to the grid using sliding mode control strategy," *Renew. Energy*, vol. 80, pp. 583–594, 2015.

[31] Wikipedia contributors, "Sliding mode control," *Wikipedia, The Free Encyclopedia*, 26-Apr-2022. [Online]. Available: https://en.wikipedia.org/w/index.php?title=Sliding_mode_control&oldid=1084772668.

[32] J.-J. E. Slotine and W. Li, *Applied nonlinear control: United States edition*. Upper Saddle River, NJ: Pearson, 1990.

[33] X. Yu, Y. Feng, and Z. Man, "Terminal sliding mode control – an overview," *IEEE Open J. Ind. Electron. Soc.*, vol. 2, pp. 36–52, 2021.

[34] Y. Tang, "Terminal sliding mode control for rigid robots," *Automatica (Oxf.)*, vol. 34, no. 1, pp. 51–56, 1998.

[35] Y. Feng, X. Yu, and Z. Man, "Non-singular adaptive terminal sliding mode control of rigid manipulators," Automatica, vol. 38, no. 12, pp. 2159–2167, 2002.

[36] X. Yu and Z. Man, "Fast terminal sliding-mode control design for nonlinear dynamical systems," IEEE Trans. Circuits Syst. I, Reg. Papers, vol. 49, no. 2, pp. 261–264, Feb. 2002.

[37] M. Zak, “Terminal attractors for addressable memory in neural network,” Phys. Lett. A, vol. 133, nos. 1/2, pp. 18–22, 1988.

[38] S. T. Venkataraman and S. Gulati, “Control of nonlinear systems using terminal sliding modes,” in Proc. Amer. Control Conf., Chicago, IL, USA, 24–26 Jun. 1992, pp. 891–893

[39] C. S. Chiu, “Derivative and integral terminal sliding mode control for a class of MIMO nonlinear systems,” Automatica, vol. 48, no. 2, pp. 316–326, 2012

[40] A. Rolan, A. Luna, G. Vazquez, D. Aguilar and G. Azevedo, "Modeling of a variable speed wind turbine with a Permanent Magnet Synchronous Generator," *2009 IEEE International Symposium on Industrial Electronics*, 2009, pp. 734-739, doi: 10.1109/ISIE.2009.5218120.

[41] 1. L. Rodriguez, 1.C. Burgos and L. Amalte. *Sistemas E6licos de Produccion de Energia Electrica.* Madrid: Editorial Rueda S.L, 2003.

[42] S. Heier, Grid Integration of Wind Energy Conversion Systems. New York: John Wiley & Sons, 1998

[43] Jou Sung-Tak, Lee Sol-Bin, Park Yong-Bae, Lee Kyo-Beum. Direct power control of a DFIG in wind turbines to improve dynamic responses. JPE September 2009;9(5):781e90

[44] A. Verma, A. Chakraborti, B. Das, P. R. Kasari, M. Mishra, and S. Pal, “A new topology for hybrid wind-solar generation system for isolated loads,” *Proc. 2018 IEEE Int. Conf. Power, Instrumentation, Control Comput. PICC 2018*, pp. 1–7, 2018

[45] R. Pena, J. C. Clare, and G. M. Asher, “Doubly fed induction generator using backto-back PWM converters and its application to variablespeed wind-energy generation,” *IEE Proc. Electr. Power Appl.*, vol. 143, no. 3, pp. 231–241, 1996

[46] M. de Prada Gil, A. Sumper, and O. Gomis-Bellmunt, “Modeling and control of a pitch-controlled variable-speed wind turbine driven by a DFIG with frequency control support in PSS/E,” in *2012 IEEE Power Electronics and Machines in Wind Applications*, 2012.

[47] B. Pavan Babu and V. Indragandhi, “Analysis of Back to Back (BTB) converter control strategies in different power system applications,” *IOP Conf. Ser. Mater. Sci. Eng.*, vol. 906, no. 1, p. 012016, 2020.

[48] “Perform transformation from three-phase (abc) signal to dq0 rotating reference frame or the inverse - Simulink,” *Mathworks.com*. [Online]. Available: https://www.mathworks.com/help/physmod/sps/powersys/ref/abctodq0dq0toabc.html. [Accessed: 21-Jun-2022].

[49] A. Pant, “Modelling and Design of Grid Connected Doubly Fed Induction Generator,” thesis, 2019.

[50] A. Dendouga, R. Abdessemed, M. L. Bendaas, and A. Chaiba, “Decoupled active and reactive power control of a doubly-fed induction generator (DFIG),” *2007 Mediterr. Conf. Control Autom. MED*, no. 1, 2007.

[51] J. Lepka and P. Stekl, “3-Phase AC Induction Motor Vector Control Using a 56F80x, 56F8100 or 56F8300 Device,” *Control*, 2001.

[52] A. Report, “Sensorless Field Oriented Control of 3-Phase Induction Motors Using Control Law Accelerator (CLA),” no. October, pp. 1–44, 2013

[53] G. Abad, *Power Electronics and Electric Drives for Traction Applications*. 2016

[54] C-S. Chiu, “Mixed feedforward/feedback based adaptive fuzzy control for a class of MIMO nonlinear systems.